

Supplementary Information for

1 **Unveiling the Methionine Cycle: A Key Metabolic Signature and *NR4A2* as a** 2 **Methionine-Responsive Oncogene in Esophageal Squamous Cell Carcinoma**

3 Xing Jin^{1,2#}, Lei Liu^{3#}, Dan Liu^{1,2#}, Jia Wu^{1,2}, Congcong Wang^{1,2}, Siliang Wang^{1,2}, Fengying Wang^{1,2},
4 Guanzhen Yu^{4,5}, Xiaoxia Jin⁶, Yu-Wen Xue⁷, Dan Jiang⁷, Yan Ni⁸, Xi Yang⁹, Ming-Song Wang¹⁰,
5 Zhi-Wei Wang¹¹, Yuriy Orlov¹²⁻¹⁶, Wei Jia¹⁷, Gerry Melino¹⁸, Ji-Bin Liu¹⁹, Wen-Lian Chen^{1,2*}.

6 *Corresponding author. Email: chenwl8412@shutcm.edu.cn (W.-L.C.)

7

8 **The supplementary file includes:**

9 **Supplementary Materials and Methods.**

10 **Figure S1. Related to Figure 1.** Activity and prognostic significance of the methionine cycle in
11 clinical ESCC tissues of patients.

12 **Figure S2. Related to Figure 1.** Increased expression of methionine transporter and metabolic
13 enzymes in clinical ESCC tissues.

14 **Figure S3. Related to Figure 2.** Exogenous SAH and Hcy uptake by ESCC cells, influence of
15 methionine and its downstream metabolites on ESCC cell growth and cell cycle progression, and
16 impact of dietary methionine on the body weight of mice.

17 **Figure S4. Related to Figure 3.** Comparison of METTL3 expression between ESCC tissues and
18 NATs from validation cohort 3.

19 **Figure S5. Related to Figure 4.** Correlation analysis between the gene expression levels in the two
20 different experimental settings, and the influence of methionine on mRNA m⁶A methylation of
21 KYSE150 cells.

22 **Figure S6. Related to Figure 5.** SAM eliciting NR4A2 expression in ESCC cells via
23 METTL3-mediated RNA m⁶A methylation, and construction of the fusion expression of wild-type or
24 mutant 3'-UTR fragment of *NR4A2* with firefly luciferase reporter.

25 **Figure S7. Related to Figure 7.** Increased expression of NR4A2 in clinical ESCC tissues.

26 **Figure S8. Related to Figure 8.** Side effect analysis of oral celecoxib administration in mice
27 harboring KYSE150 xenograft tumors.

28 **Table S1.** Basic characteristics of the discovery cohort, related to Figure 1.

29 **Table S2.** Basic characteristics of the validation cohort 1, related to Figure 1.

30 **Table S3.** Basic characteristics of the validation cohort 2, related to Figure 1.

31 **Table S4.** Basic characteristics of the validation cohort 3, related to Figure S2.

32 **Table S5.** The ingredients of high methionine (0.86%), medium methionine (0.35%), and low
33 methionine (0.17%) diets for mouse, related to Figure 2.

34

35 **Other Supplementary Materials for this manuscript includes the following:**

36 Table S6. (Excel file) RNA transcripts with modified m⁶A peaks induced by methionine, related to
37 Figure 4.

38 Uncropped WB images

39

40 **Supplementary Materials and Methods**41 **KEY RESOURCES TABLE**

REAGENT or RESOURCE	SOURCE	IDENTIFIER
Cell lines, Chemicals, Peptides, and antibodies		
Eca109	SSRCC	JY334
KYSE150	Stem Cell Bank, Chinese Academy of Sciences	TCHu236
KYSE450	Cobier Bioscience	CBP60458
KYSE30	Ek-Bioscience	CC-Y1314
Het-1A	ATCC	CRL-2692
HEK 293T	ATCC	CRL-3216
4-Nitroquinoline 1-oxide	Sigma	N8141
Methionine	MCE	HY-N0326
S-Adenosyl-L-methionine	MCE	HY-W017770
S-Adenosyl-L-Homocysteine	Solarbio	YZ-1012112
L-Homocysteine	MCE	HY-W010347
1,2-Propanediol	Sigma	57-55-6
Methylene blue	Solarbio	G1300
3-Deazaadenosine	MCE	HY-W013332A
Actinomycin D	MCE	HY-17559
STM2457	MCE	HY-134836
Celecoxib	MCE	HY-14398
Parecoxib	MCE	HY-17474A
Rofecoxib	MCE	HY-17372
Methylcellulose	MCE	HY-125861
Cycloheximide	MCE	HY-12320
Tween 80	MCE	HY-Y1891
Cisplatin	MCE	HY-17394
T-Store® Tissue Storage and Transportation Medium	Life science	TSTORE-P
Trizol	Thermo Fisher Scientific	15596018
Polybrene	Beyotime	C0351
Puromycin	Beyotime	ST551
Lipofectamine 3000	Thermo Fisher Scientific	L3000008
Lipofectamine 2000	Thermo Fisher Scientific	11668019
BsmBI	NEB	R0739S
RPMI 1640 medium	Gibco	11875093
RPMI 1640 medium (methionine-free)	BasalMedia	X102J1
penicillin-streptomycin	Gibco	15140122

REAGENT or RESOURCE	SOURCE	IDENTIFIER
Fetal Bovine Serum	Biological Industries	04-001-1ACS
Hind III	Takara	1060
XbaI	Takara	1093
PrimeSTAR® Max DNA Polymerase	Takara	R045
5×Loading buffer	Bio-rad	1610747
Anti-SLC7A5 antibody	proteintech	28670-1-AP
Anti-MAT2A antibody	proteintech	55309-1-AP
Anti-MAT2B antibody	proteintech	15952-1-AP
Anti-AHCY antibody	proteintech	10757-2-AP
Anti-Keratin 14	proteintech	10143-1-AP
Anti-Ki-67	proteintech	27309-1-AP
Anti-m ⁶ A antibody	proteintech	68055-1-Ig
Anti-NR4A2 antibody	proteintech	10975-2-AP
Anti-METTL3 antibody	Cell Signaling Technology	86132
Anti-IGF2BP1 antibody	proteintech	22803-1-AP
Anti-IGF2BP2 antibody	proteintech	11601-1-AP
Anti-IGF2BP3 antibody	proteintech	14642-1-AP
Anti- rabbit-IgG	Cell Signaling Technology	2729
Anti-Cyclin B1	proteintech	55004-1-AP
Anti-PCNA antibody	Cell Signaling Technology	13110
Anti-β-Actin antibody	proteintech	20536-1-AP
Anti-mouse-IgG-HRP antibody	Cell Signaling Technology	7076
Anti-rabbit-IgG-HRP antibody	Cell Signaling Technology	7074
Oligonucleotides (5'→3')		
CRISPR guide RNA for non-target control (NC):		
FWD: AAGAAGAATTGGGGATGATG	Addgene	N/A
REV: CATCATCCCCAATTCTTCTT		
CRISPR guide RNA #1 for human <i>METTL3</i> :		
FWD: CAGACCAGAGACTAACGAAC	Addgene	N/A
REV: GTTCGTTAGTCTCTGGTCTG		
CRISPR guide RNA #2 for human <i>METTL3</i> :		
FWD: CTTAGATCTACGGAATCCAG	Addgene	N/A
REV: CTGGATTCCGTAGATCTAAG		
CRISPR guide RNA #1 for human <i>NR4A2</i> :		
FWD: ATTACCTGTATGCTAATCGA	Addgene	N/A
REV: TCGATTAGCATAACAGGTAAT		
CRISPR guide RNA #2 for human <i>NR4A2</i> :		
FWD: TTGTCCTTCGATTAGCATAAC	Addgene	N/A
REV: GTATGCTAATCGAAGGACAA		
CRISPR guide RNA #1 for Human <i>IGF2BP2</i> :	Addgene	N/A

REAGENT or RESOURCE	SOURCE	IDENTIFIER
FWD: ACTGGCTTACCTCCCACTGC REV: GCAGTGGGAGGTAAGCCAGT		
CRISPR guide RNA #2 for Human <i>IGF2BP2</i> : FWD: ACATCCCTCCTCACCTGCAG REV: CTGCAGGTGAGGAGGGATGT	Addgene	N/A
Primers for full-length coding sequence of human <i>NR4A2</i> : FWD: CCCAAGCTTATGGACTACAAGGACGACGATGACAAGCCTTGTGTTCAGGC GCAGTATGG REV: TGCTCTAGATTAGAAAGGTAAAGTGCCAGGAAA	BioSune	N/A
Primers for <i>NR4A2</i> -Mut1: FWD: CTGCTTTTTGAATCAGCTTTCTTAGATCTGTTGTCCCTCGATTA REV: TAATCGAAGGACAAACAGATCTAAGAAAGCTGATTCAAAAAGCAG	BioSune	N/A
Primers for <i>NR4A2</i> -Mut2: FWD: CACCGCCAGCAATAATTGACAACTTTTCCTGGTCACTTTACCTT REV: AAGGTAAAGTGACCAGGAAAAGTTTGTCAATTATTGCTGGCGGTG	BioSune	N/A
Primers for <i>NR4A2</i> -3'-UTR-WT: FWD: TGCTCTAGAGACCTCCTCCCAAGCACTTCAAAGG REV: TGCTCTAGAGTGCCTATAACATTTTCAACCTAGA	BioSune	N/A
Primers for <i>NR4A2</i> -Mut3: FWD: CCCAAGCACTTCAAAGGATCTGGAATG REV: CATTCCAGATCCTTTGAAGTGCTTGGG	BioSune	N/A
Primers for qRT-PCR of <i>NR4A2</i> : FWD: GTTCAGGCGCAGTATGGGTC REV: CTCCCGAAGAGTGGTAACTGT	BioSune	N/A
Primers for qRT-PCR of <i>ACTB</i> : FWD: CATGTACGTTGCTATCCAGGC REV: CTCCTTAATGTCACGCACGAT	BioSune	N/A

Critical Commercial Assays

BCA Assay Kit	Thermo Scientific	23225
PrimeScript RT reagent Kit	Takara	RR047
FITC Annexin V Apoptosis Detection Kit	BD	556547
Cell Cycle Analysis Kit	Beyotime	C1052
Cell Counting Kit-8(CCK-8)	ShareBio	SB-CCK8
Ultrapure RNA Kit	CWBIO	CW0581
SYBR Premix Ex Taq Kit	Takara	RR390
NEBNext Poly(A) mRNA Magnetic Isolation Module	NEB	E7490
NEBNext rRNA Depletion Kit	NEB	E6310
Methylated RNA immune-precipitation (MeRIP) m ⁶ A kit	GenSeq®	GS-ET-001
QuickMutation™Plus Site-Directed Mutagenesis Kit	Beyotime	D0208S

REAGENT or RESOURCE	SOURCE	IDENTIFIER
Promega Dual-Luciferase reporter system	Promega	E1910
RNA Immunoprecipitation (RIP) kit	GenSeq®	GS-ET-006
Experimental Models: Organisms/Strains		
Mouse: BALB/c-nude	Shanghai SLAC Laboratory Animal Co.,Ltd	N/A
Mouse: C57BL/6	Shanghai SLAC Laboratory Animal Co.,Ltd	N/A
Recombinant DNA		
Lenti-CRISPR-V2	Addgene	52961
psPAX2 packaging vector	Addgene	12260
pMD2.G packaging vector	Addgene	12259
pGL3-Promoter Vector	Promega	E1761
Software and Algorithms		
R language	Open source	https://www.r-project.org/
ImageJ software	Open source	https://imagej.nih.gov/ij/
CRISPR Guide RNA database	Open source	www.addgene.org/
Autodock	Open source	autodock.scripps.edu/

42

43 RESOURCE AVAILABILITY

44 Lead contact

45 Further information and requests for resources should be directed to and will be fulfilled by the lead
46 contact, Wen-Lian Chen (chenwl8412@shutcm.edu.cn).

47 Materials availability

48 Materials and reagents used in this study are listed in the key resources table. Plasmids generated in
49 this study are available from the lead contact upon request.

50

51 Data and code availability

52 ● This paper reanalyzes the metabolomic and proteomic data of an ESCC discovery cohort which
53 we reported previously [1]. The raw data are available at <https://www.biosino.org/node> with

54 accession numbers OEP002347 for metabolomic dataset and OEP002405 for proteomic dataset.

55 ● RNA-seq and MeRIP-seq data generated by this study are deposited to the National Omics Data
56 Encyclopedia (NODE) database (<https://www.biosino.org/node>) at Bio-Med Big Data Center
57 affiliated with Shanghai Institute of Nutrition and Health, Chinese Academy of Sciences, with an
58 accession number of OEP004978.

59 ● This paper does not report original code.

60 ● Any additional information required to reanalyze the data reported in this paper is available from
61 the lead contact upon request.

62

63 **EXPERIMENTAL MODEL AND SUBJECT DETAILS**

64 **Patient cohorts**

65 We enrolled four ESCC cohorts into this study, including a discovery cohort, which we reported
66 previously [1], and three validation cohorts, from the Affiliated Tumor Hospital of Nantong
67 University (ATHNU) (Nantong, China) at different time periods: from 2013 to 2015 for validation
68 cohort 1 (n = 94), from 2019 to 2020 for validation cohort 2 (n = 112), and from 2019 to 2022 for
69 validation cohort 3 (n = 41). All patients were newly diagnosed and received no prior treatment for
70 their disease. Notably, all participants provided informed written consent in accordance with the
71 regulation of the Institutional Review Board of the ATHNU (Approval number 2019-022) in
72 agreement with the Declaration of Helsinki.

73 The following pretreatment examinations were conducted for each patient: neck, thorax, and
74 abdomen plain and contrast-enhanced computed tomography; and esophagogastroduodenoscopy,
75 with ultrasound endoscopy. Optional examinations included bronchoscopy, which was used to

76 exclude tumor infiltration into the trachea or bronchial tree, positron emission tomography, and
77 radionuclide bone imaging.

78 Disease staging was carried out according to the American Joint Committee on Cancer 8th edition
79 staging system and the Comprehensive Cancer Network (NCCN) Guidelines for Esophageal and
80 Esophagogastric Junction Cancers [2-4], while treatment protocol for each patient was established by
81 referring to the NCCN Guidelines for Esophageal and Esophagogastric Junction Cancers [3-5].

82

83 **Cellular models**

84 Human ESCC cell lines (KYSE150, Eca109, KYSE450, and KYSE30), non-transformed esophageal
85 epithelial cell line Het-1A, and HEK 293T were enrolled into this study. All cell lines were
86 authenticated using short tandem repeat (STR) profiling. Of note, all cell lines (and their derivatives)
87 were maintained in RPMI 1640 with 10% fetal bovine serum (FBS), 100 U/mL penicillin, and 100
88 mg/mL streptomycin at 37 °C in 5% CO₂.

89

90 ***Ex vivo* culture model using primary tissues from patients**

91 In the ATHNU, when the patients with ESCC underwent esophagectomy, their fresh and primary
92 tissues were quickly harvested and stored in the T-Store® Tissue Storage and Transportation Medium
93 at room temperature (RT). These fresh tissues were immediately sent to the Cancer Institute,
94 Longhua Hospital (CILH, Shanghai, China) at RT for *ex vivo* culture. The *ex vivo* culture model was
95 established as we previously described [6]. In brief, fresh tissues from patients were washed twice in
96 phosphate buffered saline (PBS) solution, cut, and weighed. Subsequently, the acquired tissue
97 segments were cultured in RPMI 1640 medium with or without methionine, as indicated in the

98 corresponding figures or figure legends.

99

100 **Mouse models**

101 A subcutaneous xenograft ESCC model and an orthotopic ESCC model induced by a chemical
102 carcinogen 4-nitroquinoline 1-oxide (4-NQO) were recruited in this study. The subcutaneous
103 xenograft tumor model was established using female BALB/c-nude mice, while the orthotopic tumor
104 model was constructed using female C57BL/6 mice. All mice were housed in well-ventilated cages
105 at a constant temperature and humidity ($23\text{ }^{\circ}\text{C} \pm 2\text{ }^{\circ}\text{C}$, 50–60%) in a specific pathogen-free (SPF)
106 controlled environment, with a standard 12-12 h light-dark cycle, and food and water were provided
107 *ad libitum*. The weight and signs of diseases were measured in regular intervals. Subcutaneous tumor
108 xenograft experiments were approved by the Institutional Animal Care and Use Committee of
109 Shanghai University of Traditional Chinese Medicine (Approval number SYXK-Hu-2020-0009).
110 Studies of carcinogen-induced ESCC mice were approved and conducted by Wuhan Servicebio
111 Technology Co., Ltd (Approval number 2018015). There were at least 5 mice in each group ($n = 5$).

112

113 **METHOD DETAILS**

114 **Acquisition of clinical specimens and clinical data**

115 In the ATHNU, ESCC tumor tissues and paired normal adjacent tissues (NATs) were harvested from
116 patients of four cohorts when they underwent esophagectomy. Tissue samples were either flash
117 frozen in liquid nitrogen and then transferred to $-80\text{ }^{\circ}\text{C}$ freezer for long-term storage, or
118 formalin-fixed paraffin-embedded for hematoxylin and eosin (H&E) staining and tissue microarray
119 preparation. The H&E slides of each patient were independently reviewed by three board-certificated

120 pathologists to assess the pathological characteristics. Acceptable ESCC tissue segments were
121 determined by the percent viable tumor nuclei (> 80%), total cellularity (> 50%) and necrosis (<
122 20%).

123 Clinical characteristics of each patient were carefully reviewed and recorded. Overall survival (OS)
124 and disease-free survival (DFS) were obtained for validation cohort 1 and validation cohort 2. OS
125 was computed using the time from the date of surgery to the date of death or the last follow-up. DFS
126 was calculated using the time from the date of resection to the date of disease recurrence or death.

127

128 **Cell culture**

129 Cells were cultured in standard RPMI 1640 or methionine-free RPMI 1640 as indicated in the figures
130 or figure legends, with 10% fetal bovine serum (FBS) or 10% dialyzed FBS (dFBS), 100 U/mL
131 penicillin, and 100 mg/mL streptomycin at 37 °C in 5% CO₂. Methionine, SAM, SAH, or Hcy was
132 supplemented into the methionine-free RPMI 1640 as demonstrated in the figures or figure legends.

133

134 ***Ex vivo* culture of primary tissues derived from patients**

135 *Ex vivo* culture of fresh and primary tissues from patients was performed following the protocol
136 which we depicted previously [6]. When the fresh tissues were received, they were washed twice in
137 PBS solution, cut, and weighed. The obtained tissue segments were cultured in methionine-free
138 RPMI 1640 medium with 10% FBS, 100 U/mL penicillin, and 100 mg/mL streptomycin at 37 °C in
139 5% CO₂ for 24 hours. Methionine, SAM, SAH, or Hcy was supplemented as indicated in the
140 corresponding figures or figure legends.

141

142 **Subcutaneous xenograft tumor mouse model**

143 For the establishment of subcutaneous xenograft model, KYSE150, Eca109, or their derivatives were
144 resuspended in PBS buffer at a density of 5×10^7 cells/mL. Subsequently, 100 μ L cell suspension
145 solution containing 5×10^6 cells was subcutaneously injected into the right flank of eight-week-old
146 female BALB/c nude mice. For the investigation of the influence of dietary methionine on
147 subcutaneous tumor growth, mice were randomly grouped as indicated in figures or figure legends
148 after 7 days of injection. Customized diets containing distinct dosage of methionine (weight/weight),
149 including 0.86% methionine (high dietary methionine), 0.35% methionine (medium dietary
150 methionine), or 0.18% methionine (low dietary methionine) (Table S5), were orally administered to
151 the corresponding groups.

152 For the investigation of the effect of celecoxib and cisplatin (CDDP) on xenograft tumor growth
153 under high dietary methionine condition, these chemical compounds were administered at day 10
154 after ESCC cell implantation using the following protocols: (1) celecoxib was prepared as a
155 suspension in 0.5% methylcellulose (w/v) and 0.1% Tween 80 (v/v) in sterile water and orally
156 administered to the mice at a dose of 25 mg/kg/day until the mice were killed; (2) CDDP was
157 dissolved in saline 0.9% solution at a dose of 2 mg/kg and intraperitoneally administered every two
158 days until the mice were killed.

159 Subcutaneous tumors were measured every three or four days using caliper. The volumes of
160 tumors were calculated using the formula $0.5 \times \text{length} \times \text{width}^2$. Mice were sacrificed three weeks
161 after cell inoculation. Xenograft tumors were harvested for imaging and weighing. Subsequently,
162 tumor tissues were flash frozen in liquid nitrogen and stored at -80 °C for further analysis.

163

164 **Carcinogen-induced ESCC mouse model**

165 An orthotopic ESCC mouse model was established by orally administering a well-known chemical
166 carcinogen 4-nitroquinoline 1-oxide (4-NQO) to six-week-old C57BL/6 female mice as we
167 previously illustrated [1, 7]. Briefly, 4-NQO stock solution was prepared in propylene glycol at 6
168 mg/mL and divided into aliquots for storage at -20 °C. Model group was constructed by orally
169 administering drinking water containing 4-NQO at a concentration of 100 µg/mL *ad libitum* for 16
170 weeks. Subsequently, model mice were randomly divided into two subgroups: one subgroup was
171 provided with pure water *ad libitum* for 12 weeks (ESCC mice), while the other subgroup was
172 supplied with water containing 10 mg/mL methionine *ad libitum* for 12 weeks (ESCC mice with Met
173 admin). Healthy control group was established by orally administering drinking water containing
174 1.67% propylene glycol (vol/vol) *ad libitum* for 16 weeks and then pure drinking water for 12 weeks.
175 At the end of the experiment, all mice were sacrificed and their esophageal tissues were collected
176 and formalin-fixed paraffin-embedded for further analysis.

177

178 **Cell viability and cell proliferation analysis**

179 Cells were cultured in standard or methionine-free RPMI 1640 medium, with 10% FBS, 100 U/mL
180 penicillin, and 100 mg/mL streptomycin at 37 °C in 5% CO₂. At the time points of cell culture as
181 indicated in the figures or figure legends, cell viability and proliferation were measured using a Cell
182 Counting Kit-8 (CCK-8) following the manufacturer's instruction.

183

184 **Cell cycle assay**

185 The following protocol was used for cell cycle assay. Cells were digested with trypsin (0.25%) and

186 washed in PBS buffer for three times. Subsequently, each cell sample was resuspended in 200 μ L
187 PBS buffer. Next, cells were fixed in ice-cold 70% ethanol for 24 hours. After incubating with
188 propidium iodide (PI)/RNase staining buffer for 30 minutes at RT, cell cycle feature of each sample
189 was measured using a flow cytometer (Beckman Coulter, DxFLEX) and analyzed using the FlowJo
190 software.

191

192 **Hematoxylin & eosin and immunohistochemistry staining**

193 Esophageal tissue samples from model mice, which were formalin-fixed paraffin-embedded, were
194 employed for hematoxylin & eosin (H&E) and immunohistochemistry (IHC) staining as we
195 previously depicted [1, 7, 8]. IHC staining was performed using antibodies against keratin-14, Ki-67,
196 and NR4A2.

197 Tissue specimens from three validation cohorts were used to construct tissue microarrays as we
198 previously described [1, 6-9]. Subsequently, tissue microarrays were stained with antibodies against
199 SLC7A5, MAT2A, MAT2B, AHCY, METTL3, and NR4A2. Quantitative staining scores of tissue
200 sections were determined by the percentage of positive cells and staining intensity. The range for
201 percentage of positive cells was from 0% to 100%. While the staining intensity was defined as 0 for
202 negative intensity, 1 for weak intensity, 2 for moderate intensity, and 3 for strong intensity. The
203 normalized staining score of each antibody of each sample was acquired by multiplying the
204 proportion value of positive cells and the intensity score of the tissue section.

205

206 **Western blot assay**

207 Supernatants of cell/tissue lysates were collected through centrifugation at $12,000 \times g$ for 10 minutes.

208 The concentrations of the supernatants containing total proteins were determined using a BCA Assay
209 Kit. Protein extracts were denatured by addition of sample loading buffer followed by boiling for 10
210 minutes. Next, proteins were separated by SDS-PAGE, and then transferred to a PVDF membrane.
211 After incubation with primary antibodies overnight at 4 °C, the membranes were washed and
212 incubated with secondary antibodies. Western blot images were captured using a ChemiDocTouch
213 Imaging System (Bio-rad).

214

215 **Quantitative reverse transcription-PCR**

216 Cell or tissue samples were lysed in Trizol reagent and total RNAs were then extracted using an
217 Ultrapure RNA Kit according to the manufacturer's recommendations. RNAs were reversely
218 transcribed to complementary DNA (cDNA) using a PrimeScript RT reagent Kit. Quantitative
219 reverse transcription-PCR (qRT-PCR) assay was performed with a SYBR Premix Ex Taq Kit on an
220 Applied Biosystems Q5 PCR machine (Applied Biosystems, Foster City, CA, USA).

221

222 **m⁶A dot blot**

223 Total RNAs were used for m⁶A dot blot assay. For cellular RNAs, cells were lysed in the Trizol
224 reagent and total RNAs were extracted using an Ultrapure RNA Kit according to the manufacturer's
225 instructions. For tissue RNAs, clinical tissue samples were cut into small pieces and homogenized in
226 the Trizol reagent on ice. Total RNAs of tissues were acquired by using the Ultrapure RNA Kit.

227 The concentrations of acquired RNA samples were determined by the NanoDrop machine. All
228 RNA samples were diluted to 400 ng/μL in RNase-free water. Next, RNA samples were denatured at
229 72 °C to disrupt their secondary structures, followed by chilling on ice immediately. Subsequently, 1

230 μ L purified RNA of each sample was dropped onto the nitrocellulose membrane, followed by
231 crosslinking in a Stratalinker 2400 UV Crosslinker in the Autocrosslink mode (1,200 microjoules,
232 25-50 seconds). After being blocked in 5% non-fat milk solution, the membranes were incubated
233 with anti-m⁶A antibody overnight at 4 °C. Finally, the membranes were washed in TBST buffer three
234 times and incubated with IgG-HRP. Dot blot images were captured by using a ChemiDocTouch
235 Imaging System (Bio-rad).

236

237 **Gene knockout by CRISPR-Cas9 approach**

238 Two human ESCC cell lines, KYSE150 and Eca109, were used for gene knockout studies according
239 to our previous protocols [1, 6, 8, 9]. Briefly, the guide RNA (gRNA) of each gene was inserted into
240 a lenti-CRISPR-V2 plasmid which was digested by the BsmBI endonuclease. The lentivirus was
241 packed as follows: lenti-CRISPR-V2 vector containing nontarget control (NC) gRNA or gRNAs of
242 target genes was co-transfected with psPAX2 and pMD2.G plasmids into HEK 293T cell using the
243 Lipofectamine 3000 reagent according to the manufacturer's recommendations. After 48 hours of
244 cell culture, the lentivirus supernatant was collected by centrifugation at 3,000 \times g and filtered using
245 a 0.45 μ m filter in order to thoroughly remove HEK 293T cells. Subsequently, ESCC cells were
246 infected with the NC lentivirus or lentivirus expressing target gRNAs in the presence of 8 μ g/mL
247 polybrene. Infected ESCC cells were screened with an antibiotic, puromycin, for 48 hours. Of note,
248 the following gRNAs were used in this study.

249 gRNA of NC: 5'-AAGAAGAATTGGGGATGATG-3';

250 gRNA#1 for *METTL3*: 5'-CAGACCAGAGACTAACGAAC-3';

251 gRNA#2 for *METTL3*: 5'-CTTAGATCTACGGAATCCAG-3';

252 gRNA#1 for *NR4A2*: 5'- ATTACCTGTATGCTAATCGA-3';
253 gRNA#2 for *NR4A2*: 5'- TTGTCCTTCGATTAGCATAAC-3';
254 gRNA#1 for *IGF2BP2*: 5'- ACTGGCTTACCTCCCCTGC-3';
255 gRNA#2 for *IGF2BP2*: 5'- ACATCCCTCCTCACCTGCAG-3'.

256

257 **NR4A2 overexpression**

258 The wild-type (WT) full-length coding sequence of *NR4A2* was cloned by a pair of primers
259 (HindIII-Flag-NR4A2-forward primer:
260 5'-CCCAAGCTTATGGACTACAAGGACGACGATGACAAGCCTTGTGTTTCAGGCGCAGTATG
261 G-3'; XbaI-NR4A2-reverse primer: 5'-TGCTCTAGATTAGAAAGGTAAAGTGTCCAGGAAA-3')
262 when using the cDNA from KYSE150 cells as the template in the presence of the PrimeSTAR® Max
263 DNA Polymerase. The sequence was then inserted into the pcDNA3.0 vector, which was
264 pre-treated with HindIII and XbaI. Next, the negative control vector pcDNA3.0 and the recombinant
265 vector pcDNA3.0-Flag-NR4A2 were transfected into ESCC cells, respectively, according to the
266 manufacturer's instructions. The transfection was performed using a Lipofectamine 3000
267 Transfection Reagent following the manufacturer's protocol.

268

269 **RNA stability assay**

270 ESCC cells were cultured in distinct media containing 5 µg/mL actinomycin D for 0 hour, 4 hours,
271 and 8 hours, respectively. Cells were lysed in the Trizol reagent and total RNAs were extracted using
272 the Ultrapure RNA Kit. Quantitative RT-PCR was conducted to measure the remaining levels of
273 *NR4A2* mRNA in cells, therefore assessing the RNA stability of *NR4A2* under different treatment

274 conditions.

275

276 **RNA immunoprecipitation assay**

277 RNA Immunoprecipitation assay (RIP) was performed using an RIP kit. Briefly, KYSE150 cells
278 were lysed in the RIP lysis buffer. The supernatant of the RIP lysate was acquired and incubated with
279 anti-IGF2BP1, anti-IGF2BP2, anti-IGF2BP3, or anti-IgG antibodies in the presence of protein A/G
280 magnetic beads under the condition of continuous shaking at 4 °C overnight. The
281 co-immunoprecipitated RNA samples were then purified with wash buffer, followed by incubation in
282 100% ethanol at -80 °C overnight. Input and co-immunoprecipitated RNAs were analyzed by
283 qRT-PCR. Finally, the enrichment of *NR4A2* by each antibody was calculated by normalizing to the
284 input *NR4A2*.

285

286 **Site-directed mutagenesis**

287 Wild-type full-length coding sequence of *NR4A2* (*NR4A2*-WT) was cloned using PrimeSTAR® Max
288 DNA Polymerase and inserted into pcDNA3.0 vector according to manufacturer's instruction. Two
289 *NR4A2* mutants with A-T substitution in exon 6 (*NR4A2*-Mut1) and exon 8 (*NR4A2*-Mut2),
290 respectively (shown in Figure 5K), were generated using the QuickMutation™Plus Site-Directed
291 Mutagenesis Kit. Briefly, different primer pairs and *NR4A2*-WT-pcDNA3.0 as a template were
292 mixed to perform PCR using BeyoAmp™ Extra-long DNA Polymerase and BeyoAmp™ Buffer.
293 PCR products were digested with DpnI enzyme and then inserted into the pcDNA3.0 vector. The
294 recombinant plasmids were transformed into *E.coli DH5a* competent cells for amplification and
295 sequencing. The primer pairs used for cloning were listed as follows.

296 Primer pair for *NR4A2*-WT:

297 Forward

298 5'-CCCAAGCTTATGGACTACAAGGACGACGATGACAAGCCTTGTGTTTCAGGCGCAGTATG

299 G-3';

300 Reverse 5'-TGCTCTAGATTAGAAAGGTAAAGTGTCCAGGAAA-3';

301 Primer pair for *NR4A2*-Mut1:

302 Forward 5'-CTGCTTTTTGAATCAGCTTTCTTAGATCTGTTTGTCTTCGATTA-3';

303 Reverse 5'-TAATCGAAGGACAAACAGATCTAAGAAAGCTGATTCAAAAAGCAG-3';

304 Primer pair for *NR4A2*-Mut2:

305 Forward 5'-CACCGCCAGCAATAATTGACAAACTTTTCCTGGTCACTTTACCTT-3';

306 Reverse 5'-AAGGTAAAGTGACCAGGAAAAGTTTGTCATTATTGCTGGCGGTG-3'.

307

308 **Dual-luciferase reporter assay**

309 Wild-type 3'-UTR fragment of *NR4A2* was cloned using the primer pair of *NR4A2*-3'-UTR-WT in
310 the presence of PrimeSTAR® Max DNA Polymerase. By using *NR4A2*-3'-UTR-WT as the template,
311 a mutant 3'-UTR of *NR4A2* (*NR4A2*-Mut3) with A-T substitution as shown in Figure 5K was
312 synthesized using a QuickMutation™Plus Site-Directed Mutagenesis Kit according to the
313 manufacturer's instructions. Furthermore, the promoter sequence of *NR4A2* was cloned using the
314 primer pair of *NR4A2*-promoter. To generate the firefly luciferase (F-luc) reporter construct,
315 *NR4A2*-3'-UTR-WT, and *NR4A2*-Mut3 were inserted into the XbaI site of the pGL3-Promoter
316 luciferase reporter plasmid, respectively. While *NR4A2*-promoter was inserted into PGL3-basic
317 luciferase reporter plasmid. Next, 50 ng recombinant luciferase reporter plasmid with

318 *NR4A2*-3'-UTR-WT, *NR4A2*-Mut3, or *NR4A2*-promoter and 50 ng TK-Renilla luciferase (R-luc)
319 control plasmids were co-transfected into HEK 293T cells using a Lipofectamine 2000 kit. F-luc and
320 R-luc activities were measured 48 hours later with the Promega Dual-Luciferase reporter system
321 (Promega, cat#E1910) according to the supplier's instructions. The relative luciferase activity was
322 computed by dividing F-luc by R-luc and normalized to individual control for each assay. The primer
323 pairs used for cloning were listed as follows.

324 Primer pair for *NR4A2*-3'-UTR-WT:

325 Forward 5'-TGCTCTAGAGACCTCCTCCCAAGCACTTCAAAGG-3';

326 Reverse 5'-TGCTCTAGAGTGCCTATAACATTTTCAACCTAGA-3';

327 Primers for *NR4A2*-Mut3:

328 Forward 5'-CCCAAGCACTTCAAAGGATCTGGAATG-3';

329 Reverse 5'-CATTCCAGATCCTTTGAAGTGCTTGGG-3';

330 Primers for *NR4A2*-promoter:

331 Forward 5'-CGGGGTACCTCCTTCTCCCCAGCTCTCCAAA-3';

332 Reverse 5'-CCCAAGCTTGGCTGGACAGGCAAAAGGGA-3'.

333

334 **Molecular docking**

335 The structure file of NR4A2 protein (ID: 5Y41) was acquired from Protein Data Bank, while the structure of
336 celecoxib was obtained from PubChem (CAS ID: 169590-42-5). NR4A2 and celecoxib were designated as the
337 receptor and ligand, respectively, to conduct molecular docking using Autodock software (version 4.2.6). The
338 docking box encompassed the entire protein as well as the ligand-receptor docking structures of NR4A2. The
339 genetic algorithm was employed with 50 semiflexible docking iterations. Other parameters of Autodock were

340 assigned at default settings. Subsequently, the LamarckianGA (4.2) option was selected to generate the
341 docking parameter file before executing Autodock program. Finally, the docking result was visualized by
342 using PyMOL (version 2.5).

343

344 **Cellular thermal shift assay (CETSA)**

345 The CETSA was performed as previously illustrated [10]. In brief, ESCC cells were incubated with
346 vehicle or celecoxib (40 μ M) for 3 hours, respectively. Cell precipitations were then acquired by
347 digestion with 0.5% trypsin. After washing twice with PBS, the cell precipitations of each group
348 were divided into 5 aliquots in PBS buffer. All cell suspensions were frozen at -80 °C and thawed for
349 three times, then sequentially incubated at 37 °C, 42 °C, 47 °C, 52 °C, and 57 °C for 3 minutes in a
350 thermal cycler, respectively. Subsequently, all cell suspensions were centrifuged at a speed of
351 12,000g at 4 °C for 10 minutes to obtain cell supernatants. NR4A2 protein levels in all samples were
352 assessed by using western blot assay.

353

354 **Untargeted metabolomic profiling**

355 Clinical tissue samples from the discovery cohort were measured using the Pegasus
356 High-Throughput Gas Chromatography with Time-of-Flight Mass Spectrometer system as we
357 previously described [1]. While clinical tissue samples from validation cohort 1 and validation cohort
358 2 were examined using the Ultra High Performance Liquid Chromatography (1290 Infinity LC,
359 Agilent Technologies) coupled to a tandem Mass Spectrometer system (TripleTOF 6600, AB Sciex)
360 (UHPLC-MS/MS) by APT Biotechnology Company (Shanghai, China).

361 **Sample preparation** A total of 206 pairs of ESCC and normal adjacent tissues from validation cohort

362 1 (n = 94) and cohort2 (n = 112) were enrolled for metabolomic profiling. Sample preparation was
363 conducted as previously illustrated [11]. Briefly, tissues were cut to pieces on dry ice and then
364 homogenized in ultrapure water. Subsequently, for each tissue sample, 200 μ L supernatant was
365 collected and thoroughly mixed with 800 μ L metabolite extraction solution (methanol/acetonitrile,
366 1:1, vol/vol), followed by centrifugation at a speed of $14,000 \times g$ at 4 °C for 20 minutes. Next, the
367 acquired supernatant was dried in vacuum centrifuge. Finally, the residual was re-dissolved in 100
368 μ L solvent (acetonitrile/water, 1:1, vol/vol), centrifuged at a speed of $14,000 \times g$ at 4°C for 20
369 minutes, and then injected for UHPLC-MS/MS analysis.

370 *UHPLC-MS/MS* Samples were separated in a hydrophilic interaction chromatography (HILIC)
371 column (2.1 mm \times 100 mm ACQUIY UPLC BEH Amide 1.7 μ m; Waters, Ireland) installed in the
372 ultra-high performance liquid chromatography system. For each sample, 2 μ L volume was injected
373 into the column at 25°C and at a flow rate of 0.5mL/min. The mobile phase, consisting of buffer A
374 (25 mM ammonium acetate and 25 mM ammonia hydroxide dissolved in ultrapure water) and buffer
375 B (acetonitrile), was employed in both ESI positive and negative modes. The gradient elution
376 procedure was set as follows: 95% buffer B for 0.5 min, linearly reduced to 65% buffer B in 6.5 min,
377 reduced to 40% buffer B in 1 min and kept for 1 min, and then increased to 95% buffer B in 0.1 min,
378 with a 3 min re-equilibration period employed.

379 The ESI source conditions were set as follows: ion source gas 1 as 60, ion source gas 2 as 60,
380 curtain gas as 30, source temperature at 600 °C, and ionspray voltage floating at \pm 5,500 V. In MS
381 only acquisition, the instrument was set to acquire over the m/z range from 60 Da to 1,000 Da, and
382 the accumulation time for TOF MS scan was set at 0.20 s/spectra. In auto MS/MS acquisition, the
383 instrument was set to acquire over the m/z range from 25 Da to 1,000 Da, and the accumulation time

384 for product ion scan was set at 0.05 s/spectra. The product ion scan was obtained using information
385 dependent acquisition with high sensitivity mode selected. The parameters were set as follows: the
386 collision energy at 35 V with ± 15 eV, de-clustering potential as 60 V (+) and -60 V (-), exclude
387 isotopes within 4 Da, and candidate ions to monitor per cycle at 10.

388

389 **Targeted metabolomic measurement**

390 ***Tissue preparation*** Frozen tissue samples stored in liquid nitrogen were taken out and accurately
391 weighed on dry ice. For each tissue sample, approximately 50 mg tissue was taken and homogenized
392 in 500 μ L organic mixture [Formic acid (FA):H₂O:Acetonitrile (ACN):Methyl alcohol (MeOH),
393 0.2:20:40:40, vol/vol/vol/vol] for metabolite extraction. The supernatant was acquired by
394 centrifugation at a speed of 13,000 rpm at 4 °C, and then stored at -80 °C for further analysis.

395 ***Medium and cell preparation*** For metabolite extraction of cell and medium samples, a mixture of
396 FA:ACN:MeOH (0.2:50:50, vol/vol/vol) and a mixture of FA:H₂O:ACN:MeOH (0.2:20:40:40,
397 vol/vol/vol/vol), which were pre-cooled at -80 °C overnight, were used as the precipitating and
398 quenching reagents, respectively. For each culture medium sample, 200 μ L of medium was added
399 into EP tube containing 800 μ L pre-cooled FA:ACN:MeOH (0.2:50:50, vol/vol/vol) and promptly
400 centrifuged at 13,000 rpm at 4°C for 15 minutes. Subsequently, 800 μ L supernatant was acquired
401 and quickly frozen at -80 °C for further analysis. For the preparation of each cell sample, spent
402 medium was discarded and culture dishes containing cells were quickly washed three times with PBS
403 buffer. Next, 1 mL of pre-cooled FA:H₂O:ACN:MeOH (0.2:20:40:40, vol/vol/vol/vol) was added
404 into each dish for rapid quenching and precipitating cell samples. After incubating at 4 °C for 15
405 minutes, cells were scraped down and then lysed by ultrasonication. Of note, during ultrasonication,

406 samples were cooled for 10 seconds on ice after every 10 seconds of ultrasonication to avoid
407 overheating. After 6 cycles of ultrasonication, lysate in culture dish was transferred into a new EP
408 tube and centrifugated at 13,000 rpm at 4 °C for 15 minutes. The acquired supernatant was stored at
409 -80 for further analysis.

410 *Standard curves for quantitative measurement of target metabolites* Standard curves were
411 established for quantitative measurement of metabolites of interest, including methionine, SAM,
412 SAH, and Hcy. To evaluate the linearity of the solutions of each standard compound, the standard
413 curve was constructed by using the concentration ratios between the compound and its corresponding
414 internal control over concentration gradient as horizontal coordinate and peak area ratios between the
415 compound and its corresponding internal control over concentration gradient as vertical coordinate,
416 and then the correlation coefficient value was calculated. Notably, correlation coefficient values for
417 all standard curves were larger than 0.99, indicating good linearity of these curves.

418 *UHPLC-MS* Samples were separated and analyzed using an ultra-high performance liquid
419 chromatography (UHPLC) (Shimadzu LC-30AD system, Shimadzu Technologies) coupled to a
420 Triple Quad 5500 Mass Spectrometer (Sciex, Applied Biosystems) by Shanghai BioNext
421 Technologies Company (Shanghai, China). A Waters ACQUITY UPLC ®BEH Amide 1.7 µm 2.1 ×
422 50 mm column was installed in the UHPLC. The composition of the mobile phase was listed as
423 follows: solution A as a water/acetonitrile solution containing 0.1% formic acid and 1 mM
424 ammonium acetate (H₂O/ACN, 95:5, vol/vol) and solution B as an acetonitrile/water solution
425 containing 0.1% formic acid and 1 mM ammonium acetate (ACN/H₂O, 95:5, vol/vol). For each
426 sample, 2 µL volume was injected into the column at 40 °C. The flow rate was set at 400 µL/min.
427 The gradient elution procedure was set as follows: 0-4 min, solution B was linearly reduced to 60%

428 from 95%; 4-5 min, buffer B was reduced to 60% from 55%; 5.0-5.1 min, buffer B was reduced to
429 50% from 55%; 5.1-5.6 min, buffer B was kept at 50%; 5.6-5.7 min, buffer B was increased to 95%
430 from 50%; 5.7-6.5 min, buffer B was kept at 95%. To detect and assess the stability and repeatability
431 of the measurement system, a set of standard curves were set at the beginning and the end of the
432 experiment, and these standard chemical samples were also used as quality controls. The standard
433 compounds in standard curves were used to correct the retention time of the chromatography.

434 Mass spectrometry analysis was performed on a Triple Quad 5500 instrument (Sciex, Applied
435 Biosystems) with ESI ion source in positive mode. The mass spectrometry parameters were set as
436 follows: source temperature at 500 °C, ion source gas 1 at 20 psi, ion source gas 2 at 20 psi, curtain
437 gas at 25 psi, ionspray voltage floating at -5,500 V. Then, the ion pairs were detected using multiple
438 reaction monitoring mode. The Q1/Q3 ion pairs for the metabolites of interest were listed as follows:
439 methionine, 150.2/132.9; SAM, 399.2/250.2; SAH, 385.3/133.6; Hcy, 136.1/55.8.

440 Peak area and retention time for each target metabolite were extracted using the Analyst software
441 (Applied Biosystems Sciex). Standard chemical compounds were used to correct the retention time
442 of peaks and identify metabolites.

443

444 **RNA-sequencing**

445 RNA-sequencing (RNA-seq) assay was performed by Cloud-Seq Biotech Inc. (Shanghai, China)
446 following our previous procedure [6]. Total RNAs were extracted from fresh frozen tissues using the
447 Trizol reagent and purified by removing rRNAs with a NEBNext[®] rRNA Depletion Kit following the
448 manufacturer's instructions. All RNA analytes were assessed for fragment size, integrity, purity and
449 concentration. Subsequently, RNA libraries were constructed using a NEBNext[®] Ultra[™] II

450 Directional RNA Library Prep Kit according to the manufacturer's instructions. Libraries were
451 controlled for quality and quantified using the Bioanalyzer 2100 system (Agilent Technologies, Inc.,
452 USA). Library sequencing was performed on an illumina Hiseq 4000 sequencer with 150 bp paired
453 end mode.

454

455 **MeRIP-sequencing**

456 Cellular mRNAs were extracted using a NEBNext Poly(A) mRNA Magnetic Isolation Module and a
457 NEBNext rRNA Depletion Kit. Fragmented RNAs (~200 nucleotides) were incubated with m⁶A
458 antibody for immunoprecipitation using a methylated RNA immunoprecipitation (MeRIP) m⁶A kit
459 according to the supplier's instructions. Both the input mRNAs without immunoprecipitation and the
460 m⁶A-immunoprecipitated mRNAs containing m⁶A peaks were used for library construction using a
461 NEBNext Ultra RNA library prep kit, and then sequenced with an Illumina NovaSeq instrument with
462 150bp paired-end reads by Cloud-Seq Biotech Ltd. Co. (Shanghai, China).

463

464 **QUANTIFICATION AND STATISTICAL ANALYSIS**

465 **Untargeted metabolomic data analysis**

466 The raw data were converted to mzXML files using ProteoWizard software, and then imported into
467 freely available XCMS software to pick peaks. During the calculation, parameters were set as
468 follows: centWave m/z = 10 ppm, peakwidth = c(10, 60), prefilter = c(10, 100). For peak grouping,
469 bw = 5, mzwid = 0.025, minfrac = 0.5. The R package, CAMERA (Collection of Algorithms of
470 MEtabolite pRofile Annotation), was applied for annotating isotopes and adducts. In the extracted
471 ion features, only the variables having more than 50% of nonzero measurement values in at least one

472 group were kept. Metabolites were identified by comparing the accuracy m/z value (<10 ppm) and
473 MS/MS spectra of peaks with an in-house database established with available authentic chemical
474 standards. Heatmaps of metabolites between two groups were generated using the R package
475 ComplexHeatmap [12].

476

477 **RNA-sequencing data analysis**

478 The quality of raw reads was assessed by Q30 values. After removing sequencing adaptors, short
479 reads (length < 35 bp) and low-quality reads with software of Cutadapt (v1.18) and Trimmomatic
480 (v0.35), high-quality clean reads were obtained. Subsequently, by using HISAT2 software (v2.1.0),
481 clean reads of human data were aligned to the human genome (assembly GRCh38). For the raw
482 count data of genes, the R package edgeR (v3.26.8) [13] was used to filter lowly expressed items and
483 to execute normalization to get reads per kilobase per million (RPKM) expression values.
484 Differentially expressed mRNAs were identified by the cuts of Benjamini-Hochberg adjusted $p <$
485 0.05 and fold change (FC) > 2 or $FC < -2$.

486

487 **MeRIP-sequencing data analysis**

488 Paired-end reads were harvested from Illumina NovaSeq 6000 sequencer. Data quality was evaluated
489 using Q30 values. The 3'-adaptors were trimmed and low-quality reads were removed using cutadapt
490 software (v1.9.3). Clean reads of all libraries were aligned to the reference genome (GRCh37/hg19 at
491 <http://genome.ucsc.edu/cgi-bin/hgGateway>) by Hisat2 software (v2.0.4). Subsequently, methylated
492 sites on RNAs (peaks) and differentially methylated sites were identified by MACS and diffReps
493 software, respectively. Differentially methylated RNA sites were identified by the cuts of $p < 0.005$

494 and $FC > 2$ or $FC < -2$. The differential peaks, overlapping with exons of mRNAs, were figured out
495 and selected by home-made scripts.

496

497 **Differential abundance scores of metabolic pathways**

498 First, all measured metabolites were mapped onto KEGG pathways. After determining which
499 metabolites were significantly increased/decreased in abundance, differential abundance (DA) scores
500 of metabolic pathways were calculated using an algorithm as depicted previously [14]. DA captures
501 the tendency for a pathway to have increased/decreased levels of metabolites, compared to a control
502 group. DA score is defined as $DA = (\text{No. of metabolites increased} - \text{no. of metabolites decreased}) /$
503 $\text{No. of measured metabolites in pathway.}$

504

505 **Prognosis-risk score of the methionine cycle metabolites**

506 To evaluate the association between the methionine cycle activity and ESCC patient prognosis, four
507 intratumoral metabolites (homocysteine, SAM, methionine, and SAH) from validation cohort 1 and
508 validation cohort 2, which are involved in the methionine cycle and presented in Figure 1D, were
509 \log_2 -transformed and then used to generate prognosis-risk score (PRS) for each patient. According
510 to the algorithm we reported previously [15], a predictive principal component analysis (PCA) model
511 was fitted in the validation cohort 1 using these four metabolites, and this PCA model was used to
512 generate PRS for each patient in validation cohort 1 and to predict PRS for each case in validation
513 cohort 2. The first principal component (a weighted average expression of four methionine cycle
514 metabolites) was employed as PRS, as it accounted for the largest variability of the data. The 70th
515 percentile of PRS values in validation cohort 1 was used as the cutoff value to divide patients from

516 validation cohort 1 and validation cohort 2 into two groups: those with low and high PRS.

517

518 **Download and analysis of the public GEO microarray dataset**

519 An GEO dataset, GSE23400, was downloaded from the NCBI Gene Expression Omnibus
520 (<http://www.ncbi.nlm.nih.gov/geo/>). This dataset was normalized using the R function `rma` in the
521 Bioconductor package `affy` and then \log_2 -transformed.

522

523 **Statistical analysis**

524 Significant differences between two groups were computed using Wilcoxon's rank-sum test for data
525 with skewed distribution or Student's t test for data with normal distribution. Survival analysis was
526 carried out by means of Kaplan-Meier method followed with log-rank test. Multivariate Cox
527 regression models were fitted using `enter` method to obtain hazard ratio values.

528 Statistical analysis was conducted with R software (R version 3.6.1, <http://www.r-project.org>).

529 All statistical tests were 2-tailed, and p values less than 0.05 were considered significant.

530

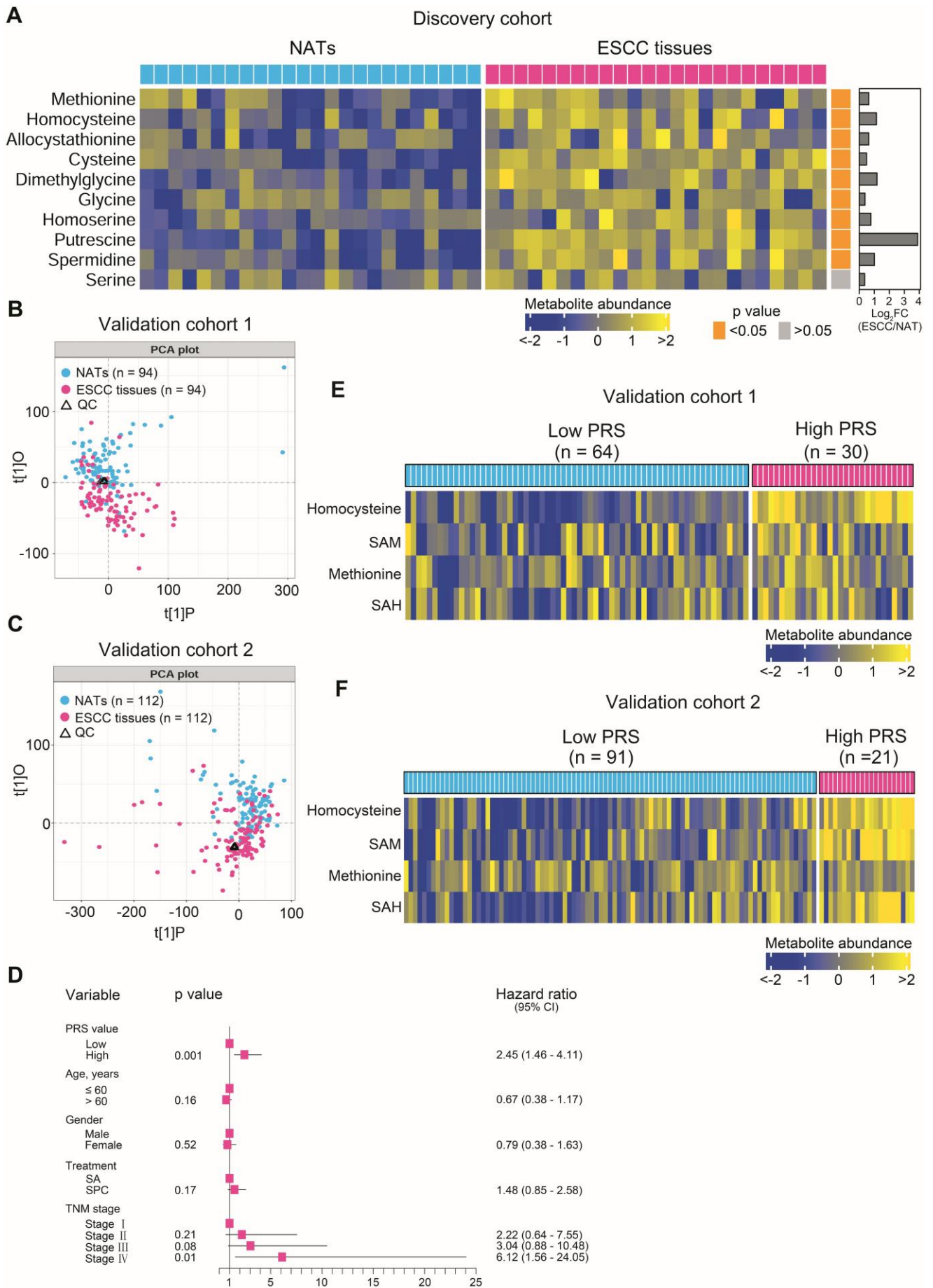
531

532 **References**

- 533 1. X. Jin, L. Liu, J. Wu, X. Jin, G. Yu, L. Jia *et al.*, A multi-omics study delineates new
534 molecular features and therapeutic targets for esophageal squamous cell carcinoma. *Clin*
535 *Transl Med* **11**, e538 (2021).
- 536 2. M. B. Amin, F. L. Greene, S. B. Edge, C. C. Compton, J. E. Gershenwald, R. K. Brookland *et*
537 *al.*, The Eighth Edition AJCC Cancer Staging Manual: Continuing to build a bridge from a
538 population-based to a more "personalized" approach to cancer staging. *CA Cancer J Clin* **67**,
539 93-99 (2017).

- 540 3. V. E. Strong, T. A. D'Amico, L. Kleinberg, J. Ajani, Impact of the 7th Edition AJCC staging
541 classification on the NCCN clinical practice guidelines in oncology for gastric and
542 esophageal cancers. *J Natl Compr Canc Netw* **11**, 60-66 (2013).
- 543 4. J. A. Ajani, T. A. D'Amico, D. J. Bentrem, J. Chao, C. Corvera, P. Das *et al.*, Esophageal and
544 Esophagogastric Junction Cancers, Version 2.2019, NCCN Clinical Practice Guidelines in
545 Oncology. *J Natl Compr Canc Netw* **17**, 855-883 (2019).
- 546 5. J. A. Ajani, T. A. D'Amico, D. J. Bentrem, D. Cooke, C. Corvera, P. Das *et al.*, Esophageal
547 and Esophagogastric Junction Cancers, Version 2.2023, NCCN Clinical Practice Guidelines
548 in Oncology. *J Natl Compr Canc Netw* **21**, 393-422 (2023).
- 549 6. W. L. Chen, X. Jin, M. Wang, D. Liu, Q. Luo, H. Tian *et al.*, GLUT5-mediated fructose
550 utilization drives lung cancer growth by stimulating fatty acid synthesis and
551 AMPK/mTORC1 signaling. *JCI Insight* **5**, (2020).
- 552 7. L. Liu, J. Wu, M. Shi, F. Wang, H. Lu, J. Liu *et al.*, New Metabolic Alterations and A
553 Predictive Marker Pipecolic Acid in Sera for Esophageal Squamous Cell Carcinoma.
554 *Genomics Proteomics Bioinformatics* **20**, 670-687 (2022).
- 555 8. D. Liu, C. Dong, F. Wang, W. Liu, X. Jin, S. L. Qi *et al.*, Active post-transcriptional
556 regulation and ACLY-mediated acetyl-CoA synthesis as a pivotal target of
557 Shuang-Huang-Sheng-Bai formula for lung adenocarcinoma treatment. *Phytomedicine* **113**,
558 154732 (2023).
- 559 9. D. Liu, X. Jin, G. Yu, M. Wang, L. Liu, W. Zhang *et al.*, Oleanolic acid blocks the purine
560 salvage pathway for cancer therapy by inactivating SOD1 and stimulating lysosomal
561 proteolysis. *Mol Ther Oncolytics* **23**, 107-123 (2021).
- 562 10. P. Luo, D. Liu, Q. Zhang, F. Yang, Y. K. Wong, F. Xia *et al.*, Celastrol induces ferroptosis in
563 activated HSCs to ameliorate hepatic fibrosis via targeting peroxiredoxins and HO-1. *Acta*
564 *Pharm Sin B* **12**, 2300-2314 (2022).

- 565 11. F. Kou, B. Zhu, W. Zhou, C. Lv, Y. Cheng, H. Wei, Targeted metabolomics reveals dynamic
566 portrayal of amino acids and derivatives in triple-negative breast cancer cells and culture
567 media. *Mol Omics* **17**, 142-152 (2021).
- 568 12. Z. Gu, R. Eils, M. Schlesner, Complex heatmaps reveal patterns and correlations in
569 multidimensional genomic data. *Bioinformatics* **32**, 2847-2849 (2016).
- 570 13. M. D. Robinson, D. J. McCarthy, G. K. Smyth, edgeR: a Bioconductor package for
571 differential expression analysis of digital gene expression data. *Bioinformatics* **26**, 139-140
572 (2010).
- 573 14. A. A. Hakimi, E. Reznik, C. H. Lee, C. J. Creighton, A. R. Brannon, A. Luna *et al.*, An
574 Integrated Metabolic Atlas of Clear Cell Renal Cell Carcinoma. *Cancer cell* **29**, 104-116
575 (2016).
- 576 15. W. L. Chen, J. H. Wang, A. H. Zhao, X. Xu, Y. H. Wang, T. L. Chen *et al.*, A distinct glucose
577 metabolism signature of acute myeloid leukemia with prognostic value. *Blood* **124**,
578 1645-1654 (2014).
- 579



581 **Figure S1. Related to Figure 1. Activity and prognostic significance of the methionine cycle in**
582 **clinical ESCC tissues of patients.**

583 (A) Comparison of the metabolites involved in methionine metabolism between tumor tissues and
584 matched NATs derived from the discovery cohort, which consisted of 24 treatment-naive patients
585 with ESCC.

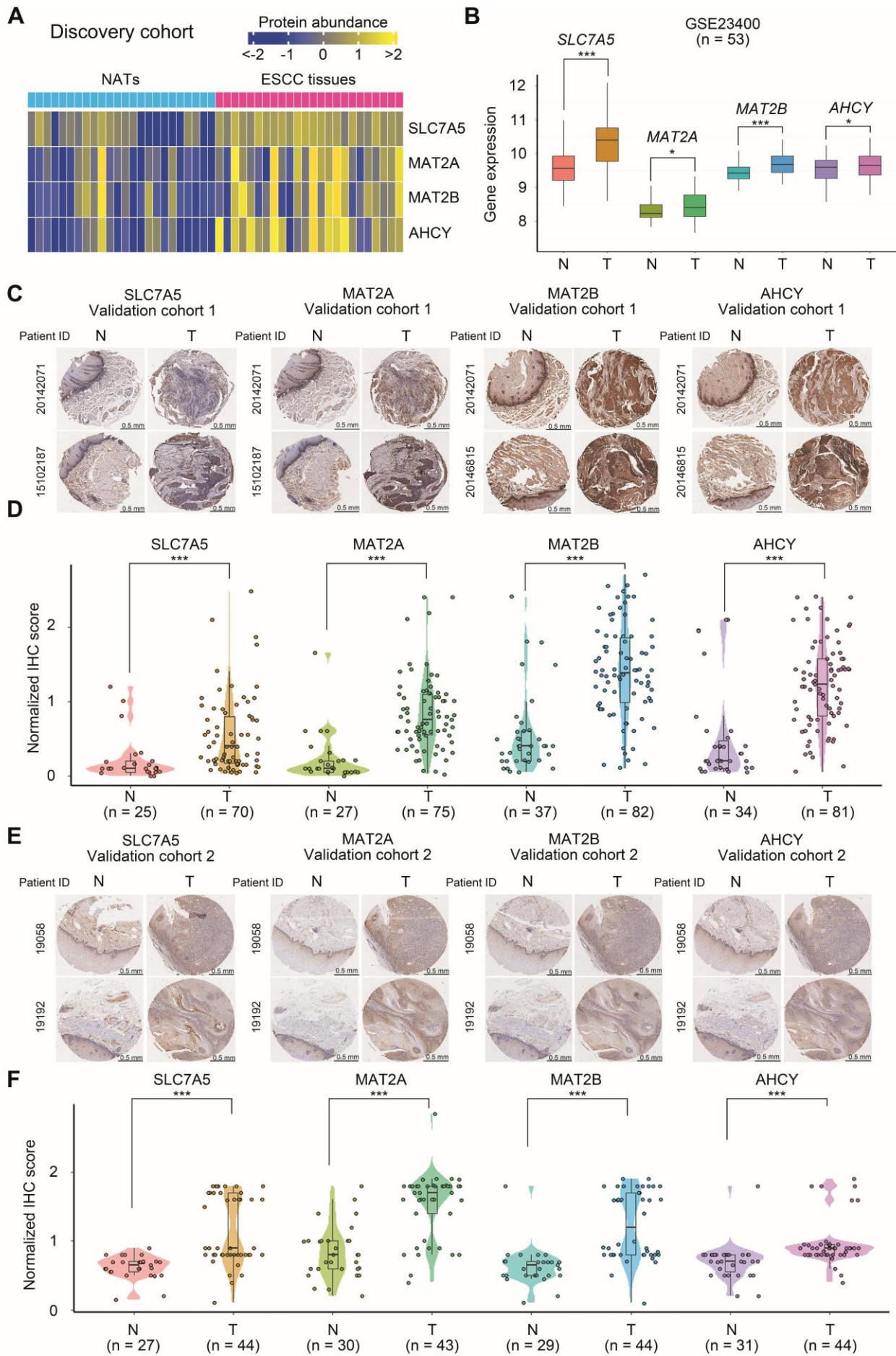
586 (B and C) PCA score plots of metabolomic data of validation cohort 1 (B) and validation cohort 2
587 (C). The quality control samples in both validation cohorts are clustered together with low dispersion,
588 indicating low systemic variation during the measurement.

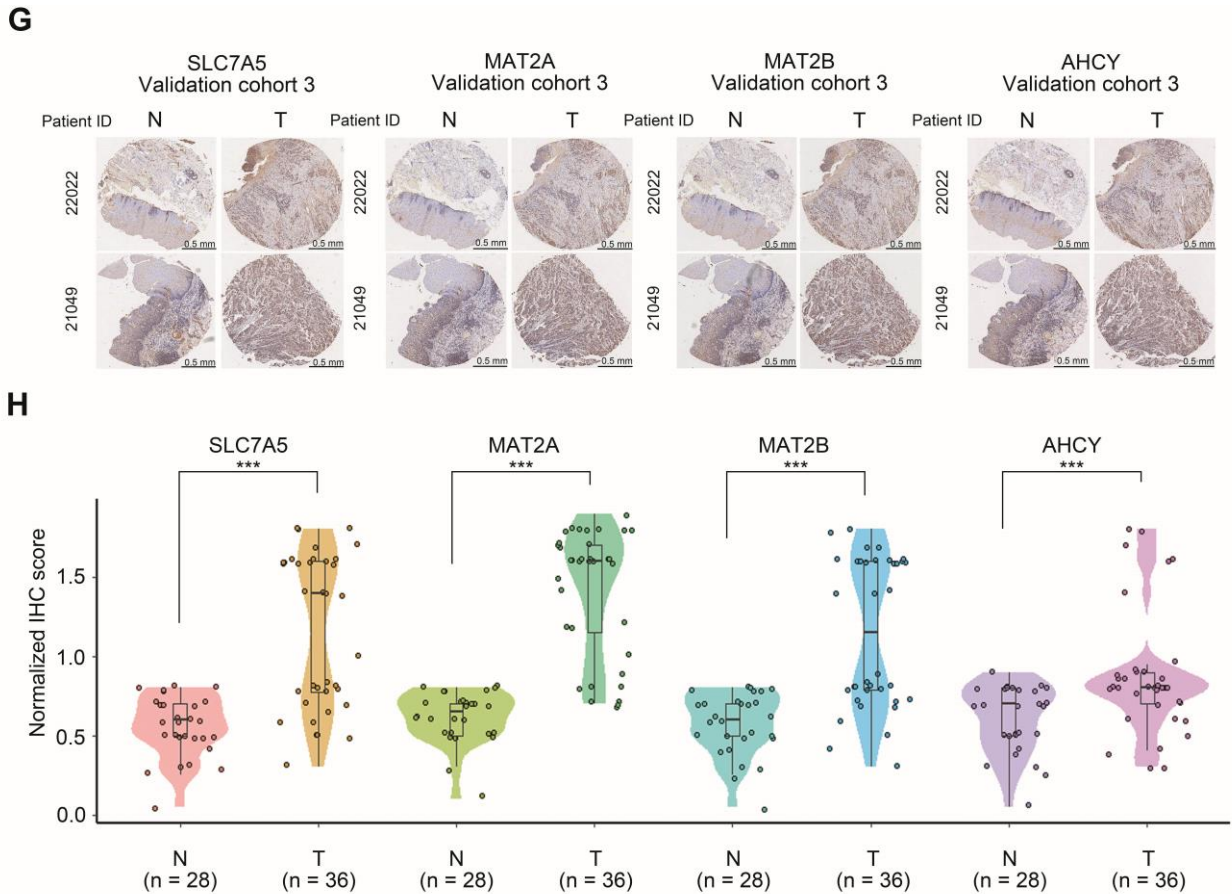
589 (D) Forest plot showing DFS hazard ratios of PRS and several well-known clinical parameters
590 derived from a multivariate Cox regression model fitted using the combined validation cohort 1 and
591 validation cohort 2.

592 (E and F) Heatmaps showing the intratumoral levels of four metabolites involved in the methionine
593 cycle between patients with high and low PRS values in validation cohort 1 (E) and validation cohort
594 2 (F).

595 ** $p < 0.01$, *** $p < 0.001$ (Wilcoxon rank-sum test).

596





598

599 **Figure S2. Related to Figure 1. Increased expression of methionine transporter and metabolic**
600 **enzymes in clinical ESCC tissues.**

601 (A) Proteomic profiling showing the protein abundance of SLC7A5, MAT2A, MAT2B, and AHCY
602 between clinical ESCC tissues and matched NATs from the discovery cohort.

603 (B) Comparison of mRNA levels of *SLC7A5*, *MAT2A*, *MAT2B*, and *AHCY* between clinical ESCC
604 tissues and matched NATs using the public gene expression dataset GSE23400.

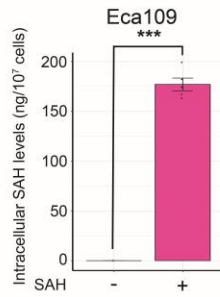
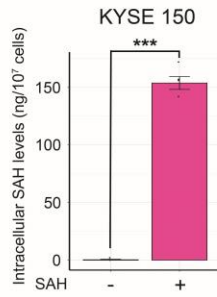
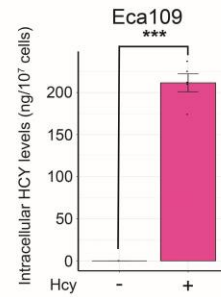
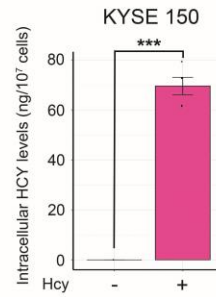
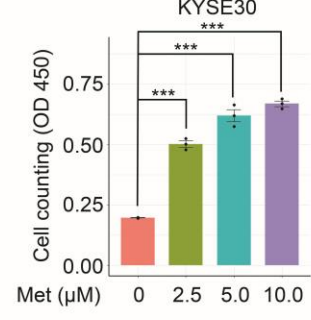
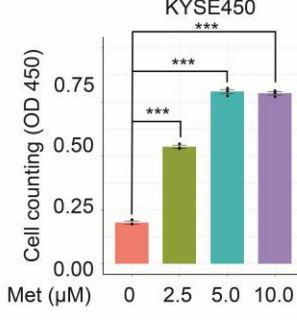
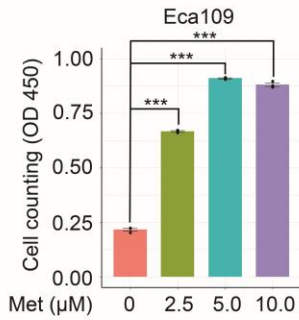
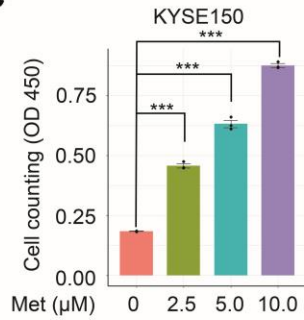
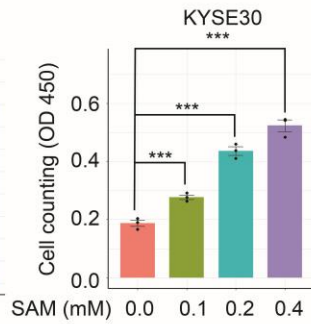
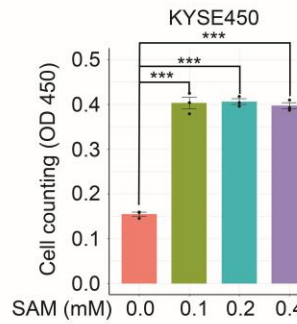
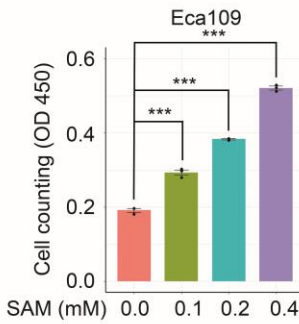
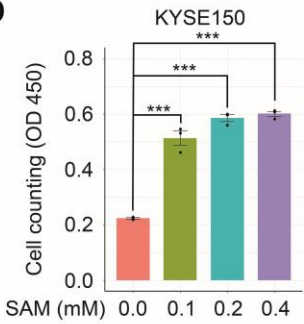
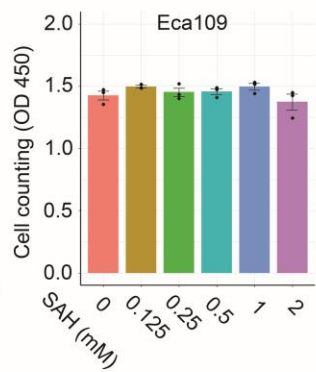
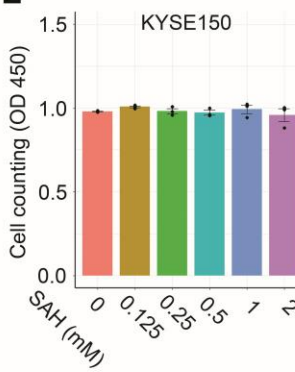
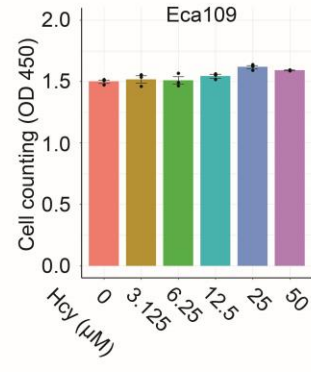
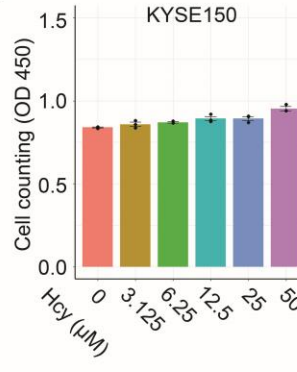
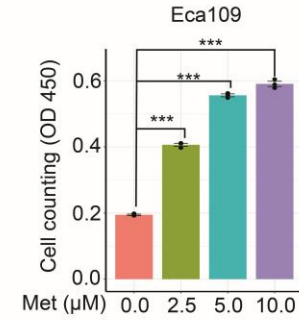
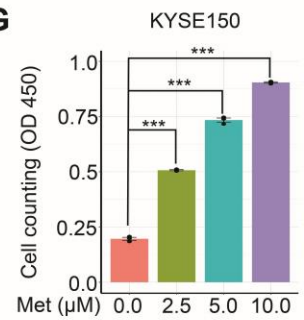
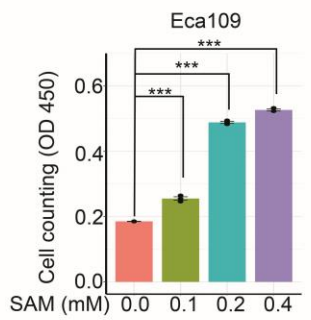
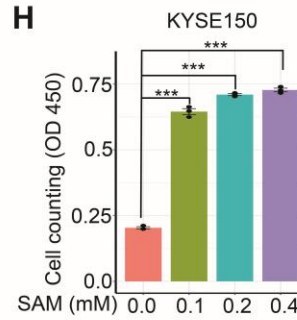
605 (C-H) Protein levels of SLC7A5, MAT2A, MAT2B, and AHCY between clinical ESCC tissues and
606 NATs derived from validation cohort 1 (C and D), validation cohort 2 (E and F) and validation cohort
607 3 (G and H), respectively. Representative IHC images (C, E and G) and statistical violin-box-scatter
608 plots (D, F and H) were presented.

609 * $p < 0.05$, *** $p < 0.001$ (Wilcoxon rank-sum test).

610

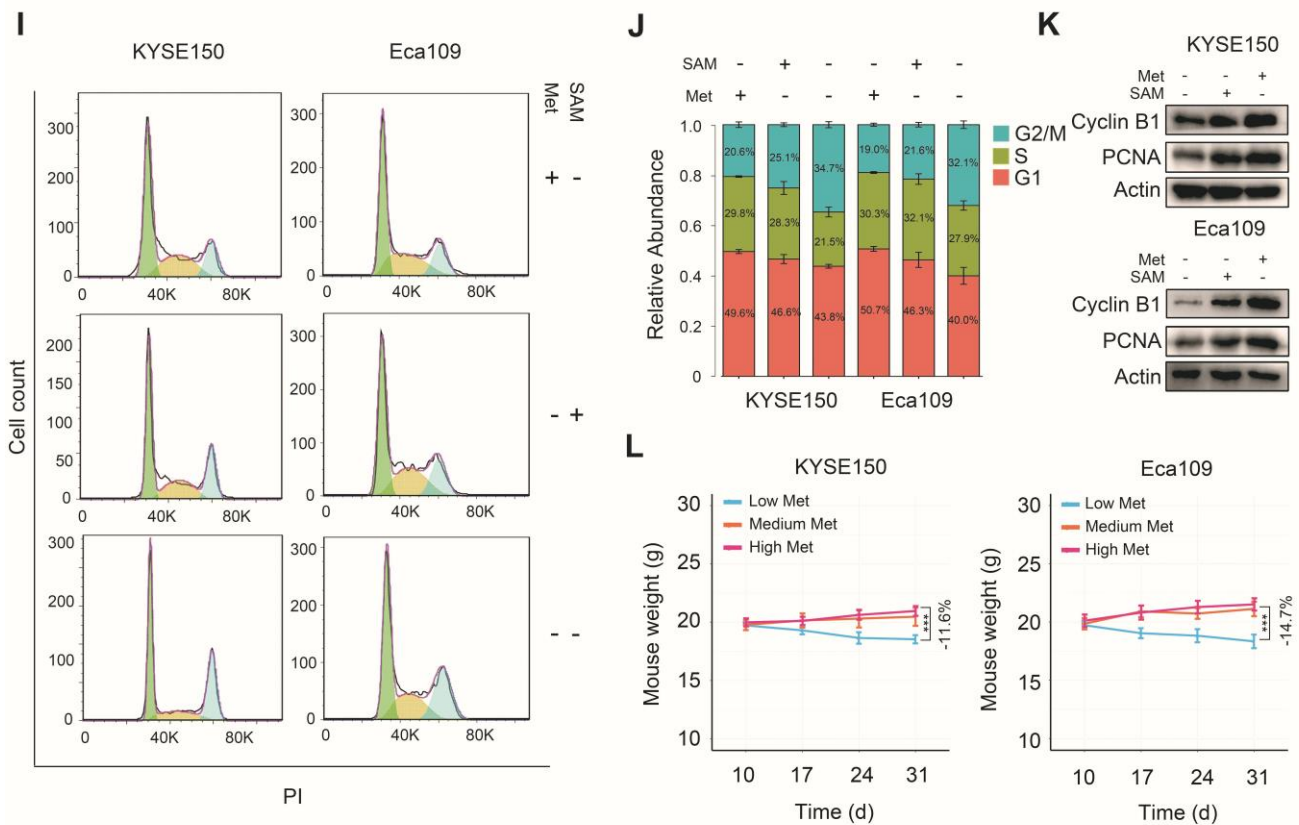
611

612

A**B****C****D****E****F****G****H**

613

614



615

616 **Figure S3. Related to Figure 2. Exogenous SAH and Hcy uptake by ESCC cells, influence of**
 617 **methionine and its downstream metabolites on ESCC cell growth and cell cycle progression,**
 618 **and impact of dietary methionine on the body weight of mice.**

619 (A and B) Comparison of intracellular SAH (C) and Hcy (D) levels between ESCC cells cultured in
 620 medium with 0.5 mM SAH or 50 μ M Hcy and methionine/SAH/Hcy-free medium for 24 hours.

621 (C-F) Methionine and SAM (C and D), but not SAH and Hcy (E and F), promoted ESCC cell
 622 proliferation in a dose-dependent manner *in vitro*.

623 (G and H) Methionine (G) and SAM (H) boosted ESCC cell propagation in a dose-dependent
 624 manner in the dialyzed medium *in vitro*.

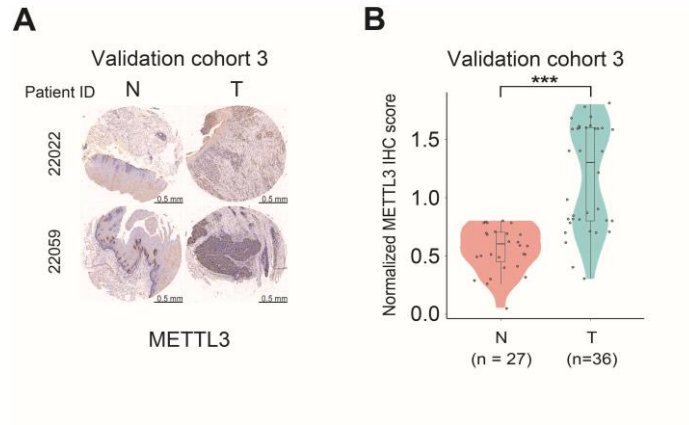
625 (I) Influence of methionine and SAM on cell cycle of ESCC cells.

626 (J) Quantification of the percentage values of ESCC cells at different cell cycle phases from (I).

627 (K) Western blot assays showing the influence of methionine and SAM on the expression of a G2/M
 628 progression marker, cyclin B1, and a cell proliferation marker PCNA.

629 (L) Impact of different levels of dietary methionine on the body weight of mice harboring
 630 subcutaneous KYSE150 or Eca109 tumors.

631 Error bars represent mean \pm SEM. * $p < 0.05$, ** $p < 0.01$, *** $p < 0.001$ (Student's t test).



632

633

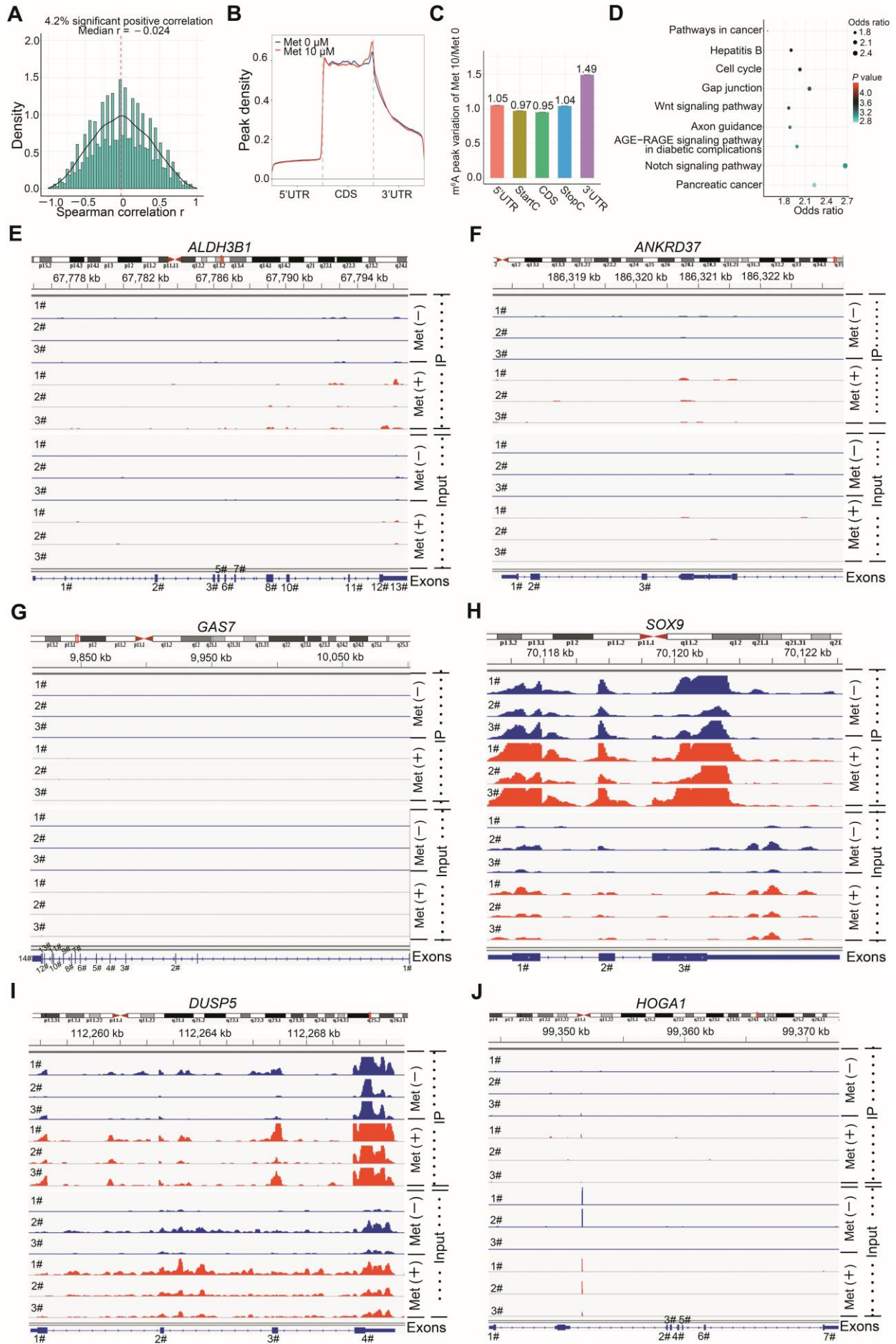
634 **Figure S4. Related to Figure 3. Comparison of METTL3 expression between ESCC tissues and**
 635 **NATs from validation cohort 3.**

636 (A) Representative IHC images.

637 (B) Statistical violin-box-scatter plots.

638 *** $p < 0.001$ (Wilcoxon rank-sum test).

639



641 **Figure S5. Related to Figure 4. Correlation analysis between the gene expression levels in the**
642 **two different experimental settings, and the influence of methionine on mRNA m⁶A**
643 **methylation of KYSE150 cells.**

644 (A) Density plot of Spearman correlation coefficient *r* values between genes in methionine-treated
645 KYSE150 cells *in vitro* and esophageal tissues from 4-NQO-induced mice with methionine
646 administration. Notably, only 4.2% of genes exhibit a significant positive correlation, and the median
647 correlation coefficient *r* value registers at a relatively low -0.24.

648 (B) Distribution of m⁶A peaks at different mRNA regions between KYSE150 cells cultured in
649 medium with 10 μM methionine and methionine-free medium.

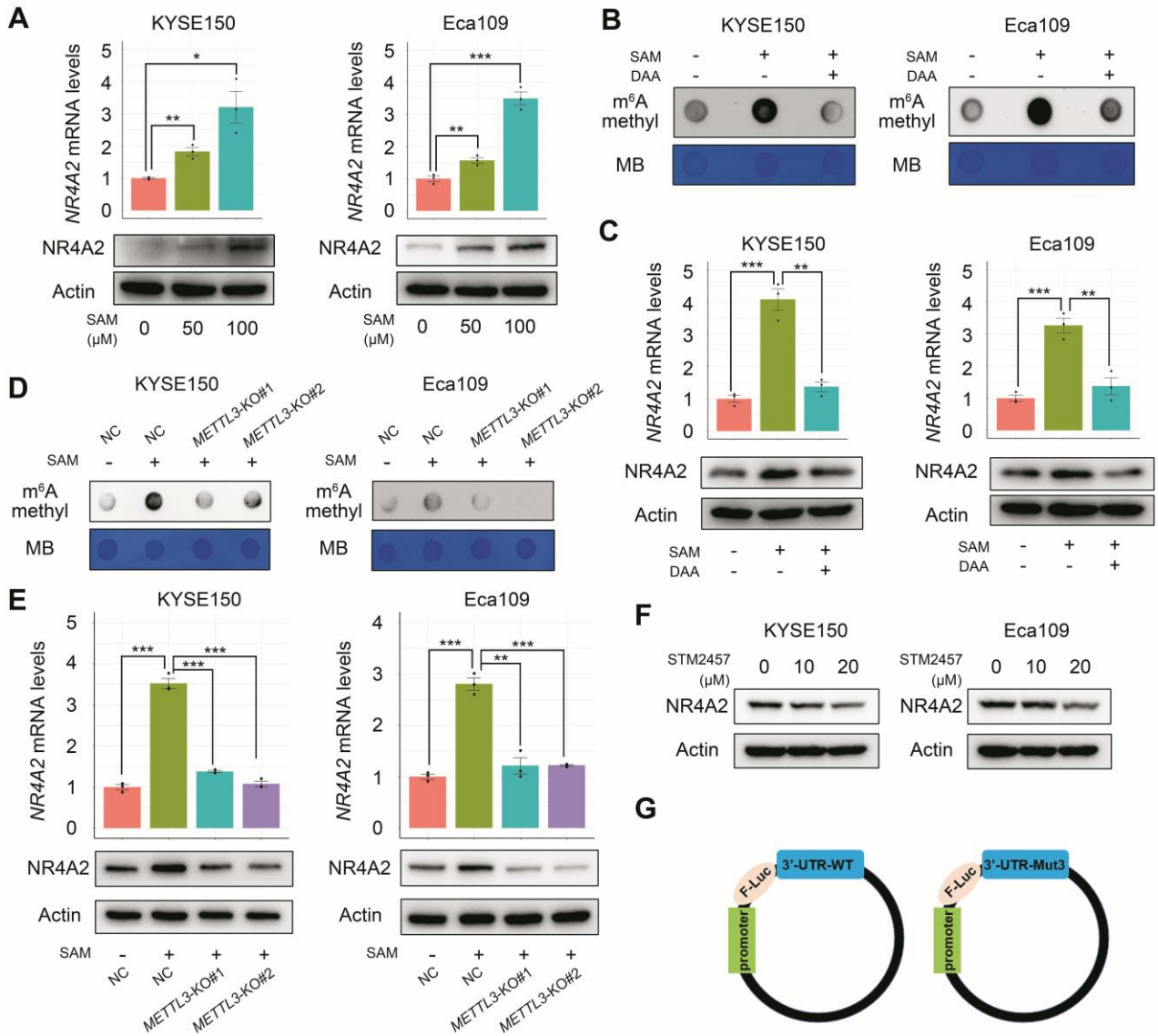
650 (C) Bar plots displaying the ratios of percentage values of m⁶A peaks at different mRNA regions in
651 KYSE150 cells. The ratio value at a specific mRNA region was calculated by dividing the
652 percentage of m⁶A peak number of KYSE150 cells treated with methionine by the percentage of m⁶A
653 peak number of KYSE150 cells treated without methionine.

654 (D) KEGG pathway enrichment analysis of gene transcripts with significantly perturbed m⁶A
655 modification.

656 (E-J) Analysis of m⁶A peaks in *ALDH3B1*, *ANKRD37*, *GAS7*, *SOX9*, *DUSP5*, and *HOGA1* mRNAs
657 between KYSE150 cells cultured in medium with 10 μM methionine and methionine-free medium.

658 UTR, untranslated regions; CDS, coding sequence.

659



661

662 **Figure S6. Related to Figure 5. SAM eliciting NR4A2 expression in ESCC cells via**
 663 **METTL3-mediated RNA m⁶A methylation, and construction of the fusion expression of**
 664 **wild-type or mutant 3'-UTR fragment of NR4A2 with firefly luciferase reporter.**

665 (A) SAM eliciting NR4A2 expression at both mRNA and protein levels in KYSE150 and Eca109
 666 cells. Cells were cultured in methionine-free medium for 24 hours.

667 (B and C) Treatment with the methylation inhibitor DAA at 10 μ M for 24 hours influencing
 668 SAM-induced RNA m⁶A methylation (B) and NR4A2 expression at both mRNA and protein levels
 669 (C) in ESCC cells. Cells were cultured in methionine-free medium.

670 (D) Impact of *METTL3* abrogation on SAM-induced RNA m⁶A methylation in ESCC cells. Cells

671 were cultured in methionine-free medium.

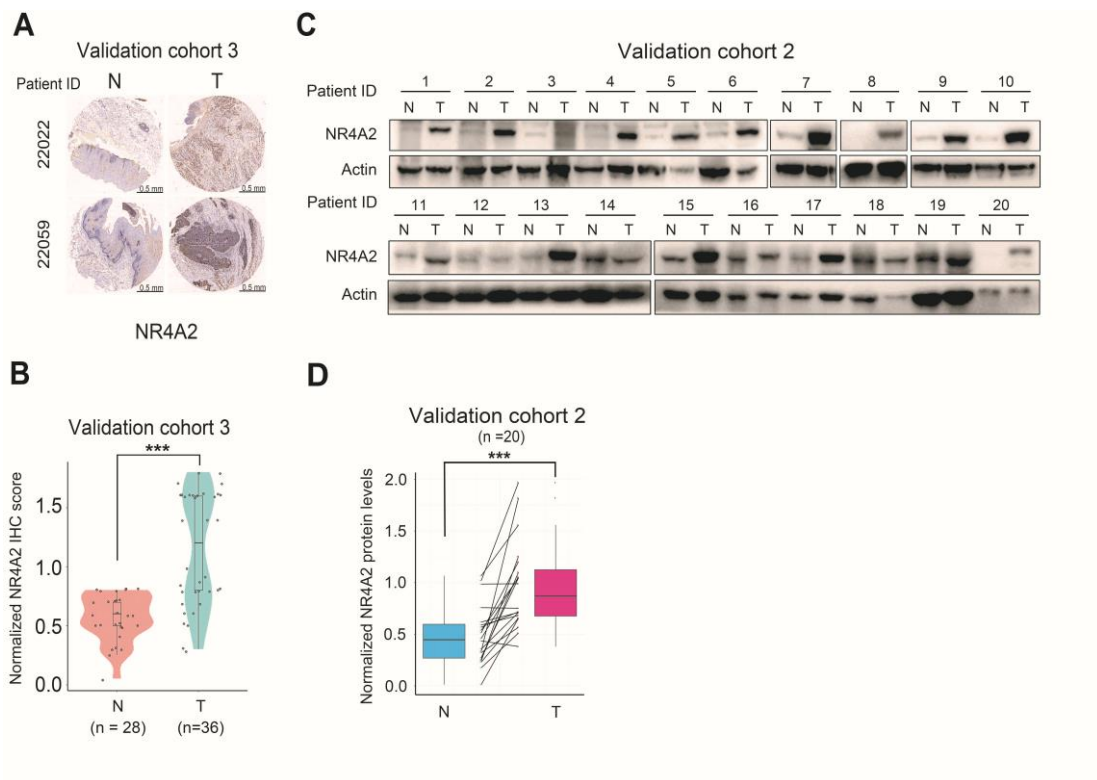
672 (E) Negative influence of SAM-induced NR4A2 expression at both mRNA and protein levels in
673 ESCC cells by *METTL3* ablation. Cells were cultured in methionine-free medium.

674 (F) Influence of STM2457 treatment on NR4A2 expression in ESCC cells. Cells were cultured in
675 complete medium.

676 (G) Schematic diagram showing the fusion of wild-type or mutant 3'-UTR fragment of *NR4A2* with
677 firefly luciferase reporter. The mutant 3'-UTR fragment contains an A-T substitution in m⁶A
678 consensus sequence as depicted in Figure 5K.

679 Error bars represent mean \pm SEM. * $p < 0.05$, ** $p < 0.01$, *** $p < 0.001$ (Student's t test).

680



681

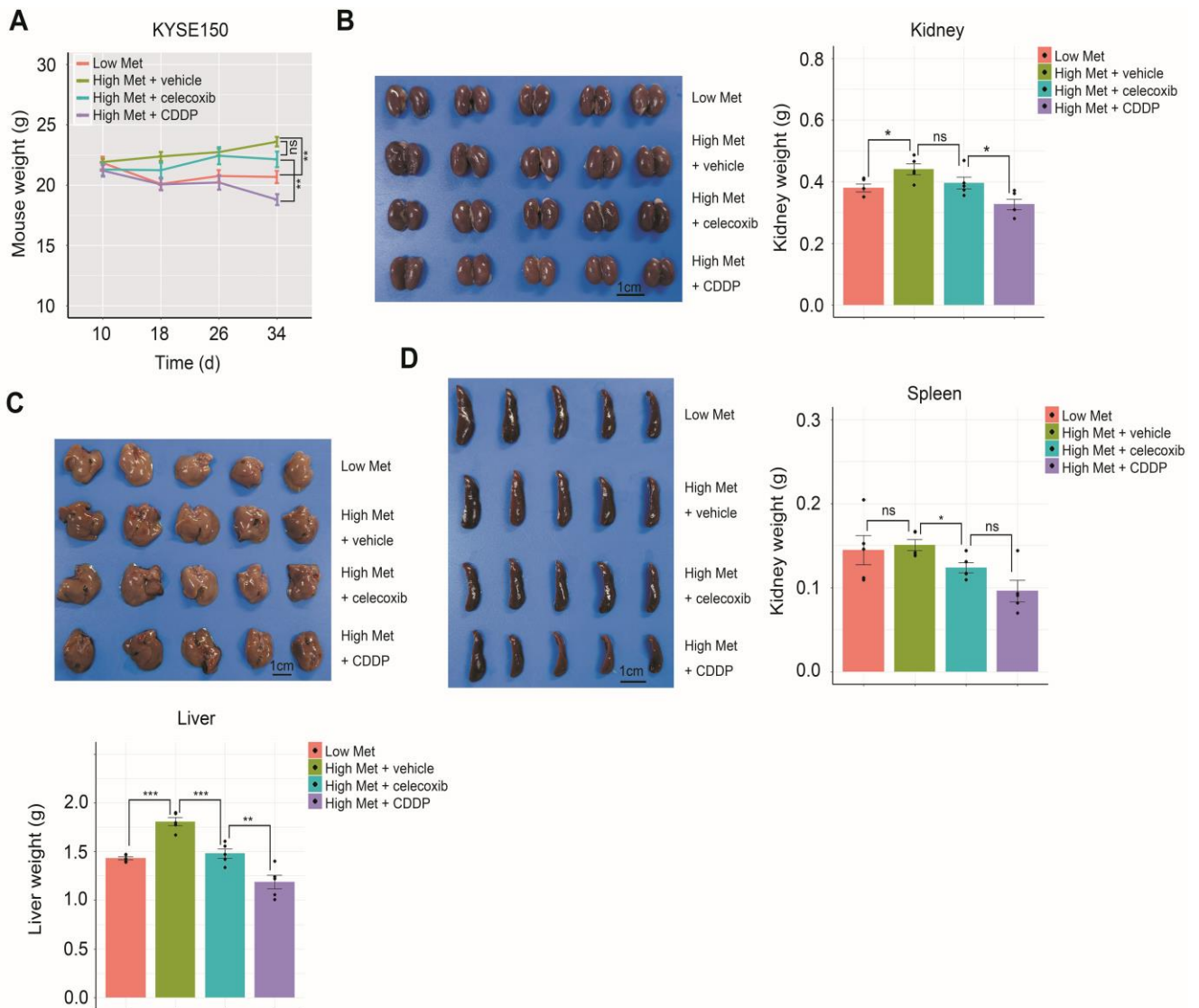
682 **Figure S7. Related to Figure 7. Increased expression of NR4A2 in clinical ESCC tissues.**

683 (A and B) IHC staining analysis comparing NR4A2 protein levels between clinical ESCC tissues and
684 NATs derived from validation cohort 3. Representative IHC images (A) and statistical
685 violin-box-scatter plots (B) are shown.

686 (C and D) Western blot assay comparing NR4A2 protein abundance between clinical ESCC tissues
687 and paired NATs derived from validation cohort 2. Statistical analysis is shown in (D).

688 *** $p < 0.001$ (Wilcoxon rank-sum test).

689



690

691 **Figure S8. Related to Figure 8. Side effect analysis of oral celecoxib administration in mice**
 692 **harboring KYSE150 xenograft tumors.**

693 (A) Comparison of the mouse weight over time among four treatment groups.

694 (B) Comparison of the kidney weight among four treatment groups.

695 (C) Comparison of the liver weight among four treatment groups.

696 (D) Comparison of the spleen weight among four treatment groups.

697 Ns, no significance.

698 Error bars represent mean \pm SEM. * $p < 0.05$, ** $p < 0.01$, *** $p < 0.001$ (Student's t test).

699

Table S1. Basic characteristics of the discovery cohort, related to Figure 1.

Characteristic	ESCC (n = 24)
Age, years	
Median (range)	68 (50-76)
≥ 60 years, no. (%)	21 (87.5)
< 60 years, no. (%)	3 (12.5)
Sex, no. (%)	
Male	15 (62.5)
Female	9 (37.5)
Alcohol consumption (habitual), no. (%)	
Never	22 (91.7)
Previous	2 (8.3)
Smoking status, no. (%)	
Never smoker	20 (83.3)
Ex-smoker	4 (16.7)
Hypertension, no. (%)	
Yes	5 (20.8)
No	19 (79.2)
Diabetes, no. (%)	
Yes	3 (12.5)
No	21 (87.5)
Histological type, no. (%)	
Squamous-cell carcinoma	24 (100)
Other	0
Treatment protocol, no. (%)	
Surgery alone	19 (79.2)
Surgery plus adjuvant chemotherapy	5 (20.8)
Clinical T stage, no. (%)	
T1	1 (4.2)
T2	3 (12.5)
T3	20 (83.3)
Clinical N stage, no. (%)	
N0	14 (58.3)
N1	8 (33.3)
N2	0
N3	2 (8.3)
Clinical stage group, no. (%)	
I	1 (4.2)
II	14 (58.3)
III	7 (29.2)
IV	2 (8.3)

Table S2. Basic characteristics of the validation cohort 1, related to Figure 1.

Characteristic	ESCC (n = 94)
Age, years	
Median (range)	64 (49-79)
≥ 60 years, no. (%)	70 (74.5)
< 60 years, no. (%)	24 (25.5)
Sex, no. (%)	
Male	71 (75.5)
Female	23 (24.5)
Alcohol consumption (habitual), no. (%)	
Never	56 (59.6)
Previous	38 (40.4)
Smoking status, no. (%)	
Never smoker	53 (56.4)
Ex-smoker	41 (43.6)
Hypertension, no. (%)	
Yes	18 (19.1)
No	76 (80.9)
Diabetes, no. (%)	
Yes	4 (4.3)
No	90 (95.7)
Histological type, no. (%)	
Squamous-cell carcinoma	94 (100)
Other	0
Treatment protocol, no. (%)	
Surgery alone	68 (72.3)
Surgery plus adjuvant chemotherapy	26 (27.7)
Clinical T stage, no. (%)	
T1	7 (7.4)
T2	24 (25.5)
T3	63 (67.0)
Clinical N stage, no. (%)	
N0	53 (56.4)
N1	26 (27.7)
N2	12 (12.8)
N3	3 (3.2)
Clinical stage group, no. (%)	
I	4 (4.3)
II	52 (55.3)
III	35 (37.2)
IV	3 (3.2)

Table S3. Basic characteristics of the validation cohort 2, related to Figure 1.

Characteristic	ESCC (n = 112)
Age, years	
Median (range)	68 (53-80)
≥60 years, no. (%)	93 (83.0)
<60 years, no. (%)	19 (17.0)
Sex, no. (%)	
Male	81 (72.3)
Female	31 (27.7)
Alcohol consumption (habitual), no. (%)	
Never	98 (87.5)
Previous	14 (12.5)
Smoking status, no. (%)	
Never smoker	76 (67.9)
Ex-smoker	36 (32.1)
Hypertension, no. (%)	
Yes	32 (28.6)
No	80 (71.4)
Diabetes, no. (%)	
Yes	13 (11.6)
No	99 (88.4)
Histological type, no. (%)	
Squamous-cell carcinoma	112 (100)
Other	0
Treatment protocol, no. (%)	
Surgery alone	73 (65.2)
Neoadjuvant chemotherapy	3 (2.7)
Surgery plus adjuvant chemotherapy	35 (31.3)
Chemotherapy only	1 (0.8)
Clinical T stage, no. (%)	
T1	16 (14.3)
T2	22 (19.6)
T3	61 (54.5)
T4	11 (9.8)
Unknow	2 (1.8)
Clinical N stage, no. (%)	
N0	58 (51.8)
N1	31 (27.7)
N2	16 (14.3)
N3	5 (4.5)
Unknow	2 (1.8)
Clinical stage group, no. (%)	
I	18 (16.1)
II	33 (29.5)

Characteristic	ESCC (n = 112)
III	46 (41.1)
IV	13 (11.6)
Unknow	2 (1.8)

707

708

Table S4. Basic characteristics of the validation cohort 3, related to Figure S2.

Characteristic	ESCC (n = 41)
Age, years	
Median (range)	66 (46-78)
≥ 60 years, no. (%)	35 (85.4)
< 60 years, no. (%)	6 (14.6)
Sex, no. (%)	
Male	27 (65.9)
Female	14 (34.1)
Alcohol consumption (habitual), no. (%)	
Never	37 (90.2)
Previous	4 (9.8)
Smoking status, no. (%)	
Never smoker	32 (78.0)
Ex-smoker	9 (22.0)
Hypertension, no. (%)	
Yes	13 (31.7)
No	28 (68.3)
Diabetes, no. (%)	
Yes	2 (4.9)
No	39 (95.1)
Histological type, no. (%)	
Squamous-cell carcinoma	41 (100)
Other	0
Treatment protocol, no. (%)	
Surgery alone	38 (92.7)
Surgery plus adjuvant chemotherapy	3 (7.3)
Clinical T stage, no. (%)	
T1	1 (2.4)
T2	10 (24.4)
T3	27 (65.9)
T4	3 (7.3)
Clinical N stage, no. (%)	
N0	16 (39.0)
N1	13 (31.7)
N2	10 (24.4)
N3	2 (4.9)
Clinical stage group, no. (%)	
I	3 (7.3)
II	25 (61.0)
III	13 (31.7)

712 **Table S5. The ingredients of high methionine (0.86%), medium methionine (0.35%), and low**
 713 **methionine (0.17%) diets for mouse, related to Figure 2.**

714 **Mouse diet with 0.86% methionine**

Ingredient	gram	kcal
Arginine	11.2	45
Glutamic Acid	27	108
Glycine	23.3	93
Histidine-HCl-H ₂ O	3.3	13
Isoleucine	8.2	33
Leucine	11.1	44
Lysine-HCl	18	72
Methionine	8.6	34
Phenylalanine	11.6	46
Threonine	8.2	33
Tryptophan	1.8	7
Valine	8.2	33
Maltodextrin	50	200
Cornstarch	432.5	1730
Dextrose	200	800
Corn Oil	80	720
Cellulose	50	0
Mineral Mix#200000	35	0
Vitamin Mix#300050	10	40
Choline Bitartrate	2	0
Yellow Dye	0.05	0

715 **Mouse diet with 0.35% methionine**

Ingredient	gram	kcal
Arginine	11.2	45
Glutamic Acid	32.1	128
Glycine	23.3	93
Histidine-HCl-H ₂ O	3.3	13
Isoleucine	8.2	33
Leucine	11.1	44
Lysine-HCl	18	72
Methionine	3.5	7
Phenylalanine	11.6	46
Threonine	8.2	33
Tryptophan	1.8	7
Valine	8.2	33
Maltodextrin	50	200

Ingredient	gram	kcal
Cornstarch	432.5	1730
Dextrose	200	800
Corn Oil	80	720
Cellulose	50	0
Mineral Mix#200000	35	0
Vitamin Mix#300050	10	40
Choline Bitartrate	2	0
Yellow Dye	0.05	0

717

718

Mouse diet with 0.17% methionine

Ingredient	gram	kcal
Arginine	11.2	45
Glutamic Acid	33.88	136
Glycine	23.3	93
Histidine-HCl-H ₂ O	3.3	13
Isoleucine	8.2	33
Leucine	11.1	44
Lysine-HCl	18	72
Methionine	1.72	7
Phenylalanine	11.6	46
Threonine	8.2	33
Tryptophan	1.8	7
Valine	8.2	33
Maltodextrin	50	200
Cornstarch	432.5	1730
Dextrose	200	800
Corn Oil	80	720
Cellulose	50	0
Mineral Mix#200000	35	0
Vitamin Mix#300050	10	40
Choline Bitartrate	2	0
Yellow Dye	0.05	0

719

720

721

722

723

724